Study on Characteristics of Sodium and Water Cavitation in Flow Contraction

Research on a Special Theme
submitted to the Tokyo Institute of Technology
for the degree of Master of Engineering

by
Teddy Ardiansyah
07M51430

Supervised by
Associate Professor Minoru Takahashi

Department of Nuclear Engineering
Graduate School of Science and Engineering
Tokyo Institute of Technology

February 10, 2009

List of Tables

List of Figures

List of Figures (continued)

List of Figures (continued)

List of Figures (continued)

List of Figures (continued)

Abstract

Cavitation experiment in flowing liquid sodium and water has been carried out. Cavitation phenomenon could occur in the liquid sodium loop of SFR in case of high sodium flow rate and low pressure. Cavitation could lead to a severe damage of the inner part of the sodium loop system, neutronic and hydrodynamic problems. The purpose of this study itself is: 1) To understand the acoustic noise and onset of water cavitation in venturi at water stagnant pressure of 0.06-0.12 MPa-a and water room temperature, and observe the phenomenon using a high-speed camera; 2) To understand the acoustic noise and onset of sodium cavitation in venturi with and without the injection of argon gas in the flowing liquid sodium at 200-400°C and stagnant pressure of 0.06-0.18 MPa-a. The test section of the experiment is a venturi with ID 6.5 mm and 20 mm in length.

Two experiments were performed for the liquid sodium cavitation, i.e. 1) without injection of argon gas into the flowing liquid sodium, and 2) with injection of argon gas into the flowing liquid sodium. The experiments were conducted at liquid sodium temperature of 200-400°C and stagnant pressure of 0.06-0.18 MPa-a. The results show that the formation and collapse of cavitation bubbles produced very high noise intensity recorded by accelerometer placed on the test section at high temperature. At developed cavitation condition, the noise intensity becomes saturated. The injection of argon gas into the flowing liquid sodium does not affect the noise intensity during cavitation which might be explained by the change in bubbles size and shape when they grew and passed through the venturi and collapsed at the downstream region. The onset cavitation coefficient K for sodium cavitation is close to the theoretical value of unity.

For the water cavitation experiment, the results show that the noise intensity during cavitation condition in water is a little bit lower compared to that in liquid sodium because sound travels more easily in liquid sodium than in water. Also, the test section part in water does not have wave guide rod which can attenuate the signal. For both experiments (sodium and water cavitations), the increase of the stagnant pressure and temperature affects the flow rate to start cavitation inception in the test section. It indicates that at high pressure condition, the formation of cavitation bubbles is suppressed and cavitation starts to occur at lower cavitation coefficient and higher velocity. But the change of stagnant pressure and temperature do not affect the magnitude of the noise intensity produced during cavitation conditions. The noise intensity tends to increase at higher frequency region at low temperature, but increase in both high and low frequency regions at high temperature. Observation of cavitation phenomenon in water using a high speed camera at 8,000 fps showed that most of the bubbles that collapsed at the downstream region were not spherical and the collapse was observed far away from the venturi outlet. The non-spherical bubbles might be affected by the pressure gradient, boundary layers, turbulence and the collapse of other bubbles. The phenomenon similar to the critical/choked flow phenomenon was observed during developed cavitation condition in liquid sodium, but not in water.

Keywords: cavitation, sodium, water, noise, venturi.

CHAPTER I

Introduction

1.1. Background

1.1.1. World energy demand

The world energy demand has been increasing in the last few years. According to the projection of the International Energy Agency (IEA) in its World Energy Outlook 2008 [1], the demand of primary energy grows by 1.6% per year on average in 2006-2030. This demand will certainly require a lot of energy supply from various sources. Oil, gas and coal are still the major energy sources for the present condition, but the demand of more cleaner, sustainable, affordable and cost-effective energy sources is getting more popular these days. One of the options being considered is nuclear energy. Nuclear energy plays a vital role to cut the greenhouse effects [2]. At present, there are total of 438 nuclear power plants under operation worldwide [3], and nuclear share of the world electricity in 2005 is about 16% [2].

1.1.2. Development of nuclear power plants

The development of nuclear power plants dated back as far as 1940s when Enrico Fermi succeeded to sustain the first fission reaction at the University of Chicago. This marked the beginning era of nuclear energy as one of the primary energy sources to support human life on earth. The first generation of nuclear reactors (known as Generation I) was advanced in 1960s and 1970s in the early prototype reactors, such as Shippingport, Dresden, Fermi I and Magnox. Some of these reactors were then developed into commercial ones in 1970s in the type of light water reactors (LWRs), such as pressurized water reactors (PWRs) and boiling water reactors (BWRs); heavy water reactors (HWRs), such as Canada Deuterium Uranium (CANDU); or gas, such as advanced gas-cooled reactors (AGRs). This kind of nuclear reactors were known to be as Generation II nuclear reactors. The development later continued to the Generation III in 1990s with the improvement of the previous Generation II reactors, such as improved fuel technology, passive safety systems and the lifetime of operations. Some of the Generation III reactors have been built and operated such as advanced boiling water reactors (ABWRs) in Japan, System 80+ and advance pressurized water reactors (APRs). Further advances of the Generation III reactors are underway and are actively being developed. This Generation III+ offers evolutionary designs to improve economics for near-term deployment. The long-term deployable plants (known as Generation IV) are now being researched intensively in several countries, such as Japan, the United States and Russia. All of the Generation IV reactors must meet eight primary goals listed in the Generation IV roadmap, i.e. improve nuclear safety, minimize waste and resource utilization, highly economical, proliferation resistance and physical resistance against acts of terrorism. Examples are sodium-cooled fast reactor (SFR), very high temperature reactor (VHTR), supercritical water-cooled reactor (SCWR), molten salt reactor (MSR), gas-cooled fast reactor (GFR) and Lead-cooled fast reactor (LFR) [4]. According to IAEA in 2007 the uranium availability for nuclear powers can be extended from 85 to 5,000-6,000 years by fast reactor fuel cycle with recycling using identified uranium resources [5].

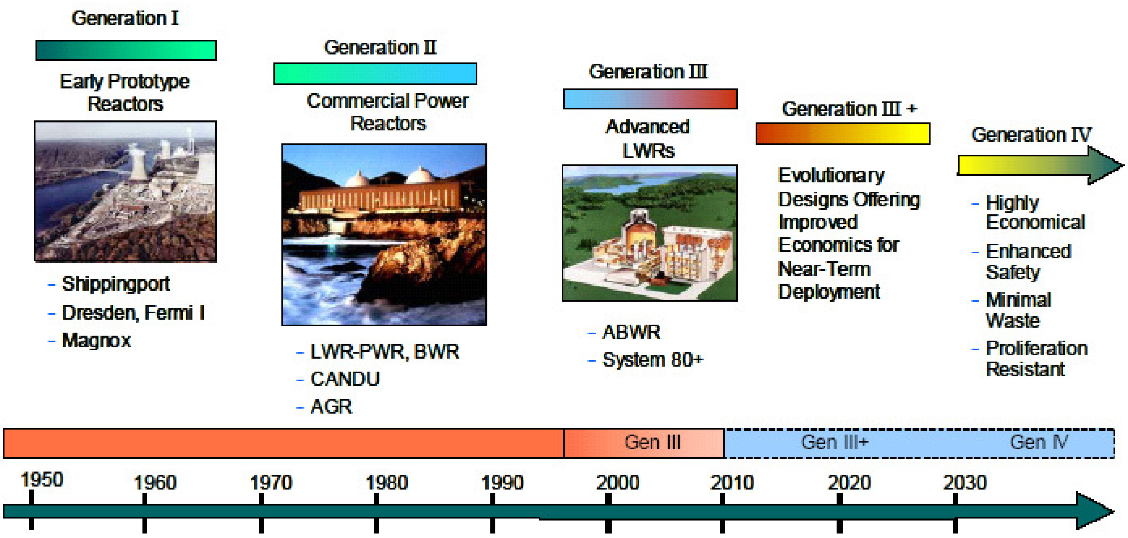

Fig. 1-1. Technology roadmap of nuclear power plants [4]

1.1.3. Sodium-cooled fast reactor (SFR)

The sodium-cooled fast reactor (SFR) is one of the Generation IV projects of fast reactors. The main concept of the SFR is to utilize the fast neutron spectrums using a closed fuel cycle with full actinide recycle [6] hence, increase the lifetime of uranium resources as well as to produce electricity. To achieve this condition, sodium is used as the main coolant in the reactor core. The advantages of sodium over other coolants are higher thermal conductivity to achieve higher reactor power efficiency, higher boiling point at atmospheric condition compared with water, low moderation to fast neutrons and non-corrosive to reactor metal structures. The disadvantages of the sodium are it will react violently in contact with water or air, creating fire. According to the concept outlined by the Generation IV International Forum (GIF), the SFR is top-ranked in sustainability because of its closed-fuel cycle and actinide management. There are two options envisioned for actinide recycle in SFR: one using intermediate size (150 to 500 MWe) with uranium-plutonium-minor-actinide-zirconium metal alloy fuel and the other one using medium to large size (500 to 1500 MWe) with mixed uranium-plutonium oxide fuel. The SFR will be operated approximately at 550°C [4]. In Japan itself, the SFR have been developed and researched extensively. This has been realized by the development of experimental fast reactor JOYO and MONJU.

Experimental fast reactor JOYO is an important step in the fast breeder reactor (FBR) development program in Japan. The three major objectives of JOYO are to advance the technology thorough operation and experiment, to conduct irradiation test of fuel and materials and to validate the innovative technology for future FBR program in Japan. JOYO is operated with thermal power of 140 MWt. The coolant inlet and outlet temperature are 350° and 500°C, respectively. The sodium coolant flow rate of JOYO is around 2,700 ton/h.

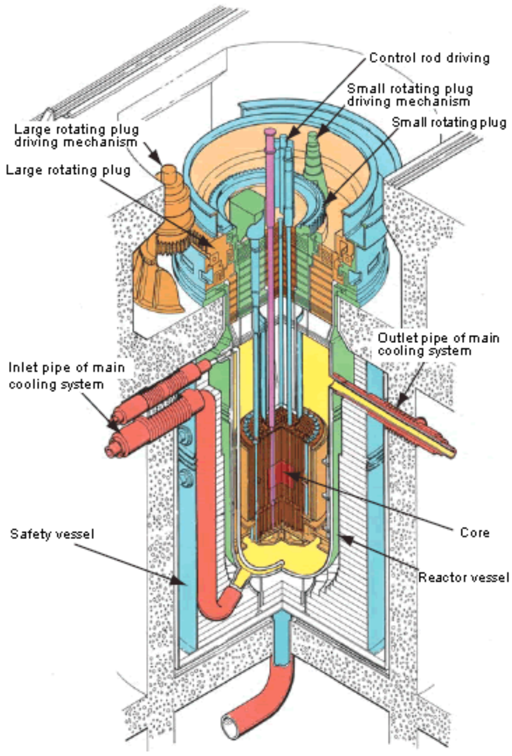

Fig. 1-2. Cutaway of the JOYO reactor core and surroundings

MONJU in the other hand is the first Japan`s prototype of FBR. It is constructed in Tsuruga City, Fukui prefecture. The liquid sodium inlet and outlet temperature of MONJU are 397° and 529°C in the primary system, and 325° and 505°C in the secondary system, respectively. Due to sodium leak in 1995, MONJU has been shut down until future notice and completed a lot of modification works in May 2007. According to M. H. Chang in the 4th Tsuruga International Energy Forum 2004 [7], MONJU is a valuable asset not just for Japan but also for the whole world with respect to fast reactor technology development and the restart of MONJU is vital for the early commercialization of FBR in the future.

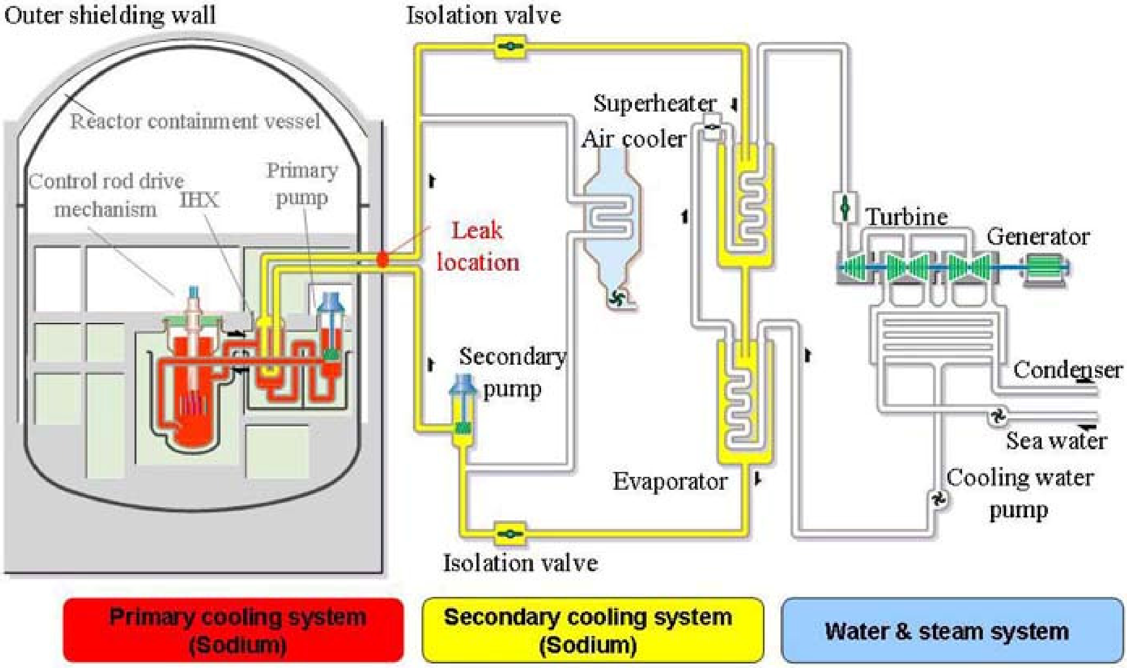

Fig. 1-3. Overview of MONJU

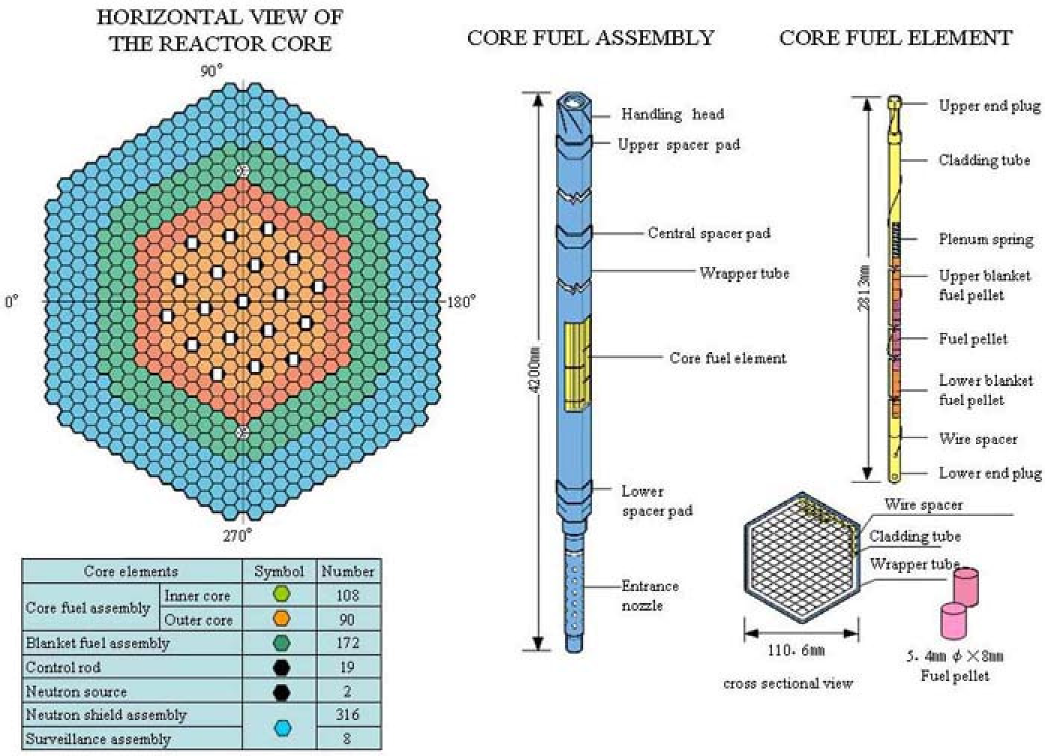

Core elements		Symbol	Number
Core fuel assembly	Inner core		108
	Outer core		90
Blanket fuel assembly			172
Control rod			19
Neutron source			2
Neutron shield assembly			316
Surveillance assembly			8

Fig. 1-4. Reactor core structure of MONJU

1.2. Cavitation Phenomenon in SFR

Cavitation phenomenon could occur in the liquid sodium loop due to the high sodium flow rate. The possible regions where cavitation could occur are at the fuel assembly entrance nozzle in the connecting tube, the gap between support plate and fuel assembly, upper and lower neutron shield, orifices between high pressure plenum and low pressure plenum, elbow and suction pipe. The occurrences of cavitation could lead to a severe damage to the inner part of the sodium loop system and metal fatigue of the piping systems due to vibrations caused by cavitation bubbles. The damages can lead to a severe accident in the reactor plant and endanger not only the lives of the plant's personnel but also the surrounding community.

1.3. Previous Study

Previous study related to cavitation has been conducted by several researchers. P. Courbiere [8] conducted an experiment on cavitation in orifice and pumps with sodium and water. He found that the similitude between water and sodium cavitation is satisfactory as long as the entrained gas volume in the sodium remains below 10^{-5}, and the water is unsaturated and degassed. S. R. Bistafa [9] conducted another experiment with different air concentration in water and stated that air content effects are significant in cavitation. Other researchers measured the noise generated by the collapse of cavitation bubbles such as by P. Testud et al and S. L. Ceccio et al [10, 11]. The collapse of the cavitation bubbles could have significant effect to the damage of materials as observed by S. G. Young et al [12]. In case of complex system, the observation of cavitation phenomenon is rather difficult and some indirect methods could be used to detect its occurance, such as by using high speed pressure transducer and accelerometer, monitoring of acoustic pressure emission using microphone and sound level meter, and flow (visual) observation using camera [13].

1.4. Purpose of Study

The purpose of the study is:

1) To understand the acoustic noise and onset of sodium cavitation in venturi with and without the injection of argon gas in the flowing liquid sodium at 200-400°C, and stagnant pressure of 0.06-0.18 MPa-a.
2) To understand the acoustic noise and onset of water cavitation in venturi at water stagnant pressure of 0.06-0.12 MPa-a and water room temperature (10.2-17.6°C), and observe the phenomenon using a high-speed camera.

CHAPTER II

Experimental Apparatus and Procedure

2.1. Experimental Apparatus

2.1.1. Description of Sodium Loop Test Apparatus

Liquid sodium cavitation experiment was conducted using a sodium loop facility at Sukegawa Electric Co., Ltd. shown in Fig. 1. This sodium loop facility can be operated up to 500°C and maximum sodium flow rate of 20 L/min. It consists of a test section, an electromagnetic pump (EMP), two electromagnetic flow rate meters (EMFs), a heater, a cooler, a cold trap and an expansion tank. The heater and expansion tank control the temperature and the stagnant pressure of the sodium loop at the required experimental conditions, respectively. Argon gas was used as cover gas inside the expansion tank. The flow rate of the liquid sodium was measured using the EMF at the bottom part of the loop. For the purpose of this experiment, the cold trap and EMF-2 shown by the green lines were not used.

The test section of the loop was made from SS-316. It consists of a gas injector, a venturi, a wave guide rod and a static pressure tap. A gas injector is mounted at the test section to inject argon gas in the flowing liquid sodium. The venturi is used to create cavitation bubbles inside the liquid sodium that passes through it. The acoustics noise signals generated from the cavitation bubbles were measured by using an accelerometer (Ono Sokki NP-2710) installed at the bottom part of the wave guide rod. Ono Sokki NP-2710 accelerometer is a piezoelectric accelerometer and seismic vibration detector, and therefore do not require a reference point for measurement. The measurement can be performed easily just by attaching the accelerometer to the test object. In piezoelectric element, when force is applied to a single crystal or to barium titanate, an electric charge is generated on its surface. According to the method of applying force to the piezoelectric element, Ono Sokki NP-2710 is a shear-type accelerometer. With the shear type, an electrical charge is generated when force is applied to the piezoelectric element in the shear directions [14]. The downstream pressure of the test section was measured by using a pressure transducer (Ashcroft GC-51) connected to the pressure tap.

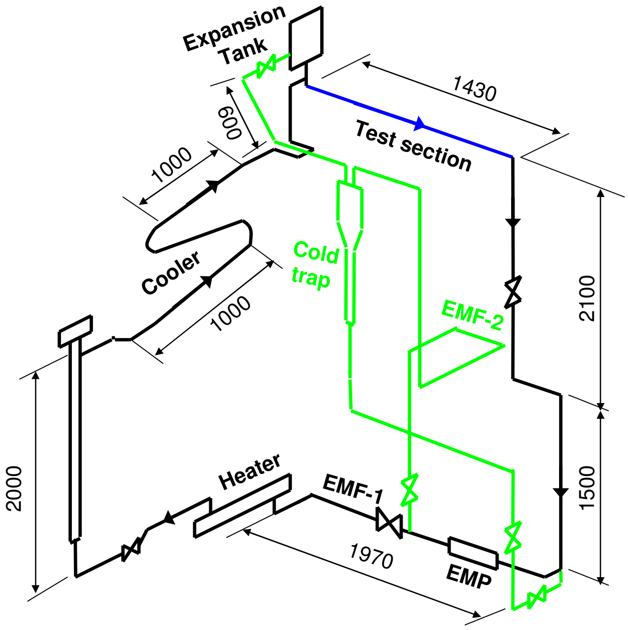

Fig. 2-1. Schematic of the sodium loop facility

In order to obtain the high flow rate necessary to generate cavitation conditions inside the liquid sodium, the inner diameter of the venturi is reduced to 6.5 mm with the maximum sodium flow rate of 20 L/min. The choice of 6.5 mm inner diameter of the venturi is to offset between the effect of the pressure drops along the liquid sodium test section part and the pump head of the electromagnetic pump. The pressure drops along the test section were calculated analytically using the following formula:

$$\Delta p = (K_c + K_e)\frac{\rho}{2}V_0^2 + \frac{0.3164}{\mathrm{Re}^{0.25}}\frac{\rho}{2}V_1^2\frac{L}{D1} \qquad (1)$$

where Δp is the pressure drop along the test section part, K_c is the contraction coefficient, K_e is the enlargement coefficient, ρ is the sodium density, V_0 is the sodium velocity at venturi part, V_1 is the sodium velocity at downstream region, Re is the Reynold`s number, L is the length of the test section, and D_1 is the inner diameter of the downstream region.

This equation above is derived from incompressible flow moving from point A to B along a pipe,

$$\Delta p = \rho g\left(\Delta z + f\frac{L}{D}\frac{V^2}{2g}\right) \qquad (2)$$

Where Δz is change in pipe elevation, f is the friction factor, L is the length of the pipe, D is the pipe diameter, and g is the gravity constant. For smooth pipes, Blausisus suggests, for Reynolds`s numbers between 3000 and 100,000 [15],

$$f = \frac{0.316}{\mathrm{Re}^{0.25}} \tag{3}$$

And for the contraction and enlargement part of the venturi, the pressure drop can be written as,

$$(K_c + K_e)\frac{\rho}{2}V^2 \tag{4}$$

Summing up equation equation (2), (3) and (4) we can solve the pressure drop along the test section as indicated by equation (1).

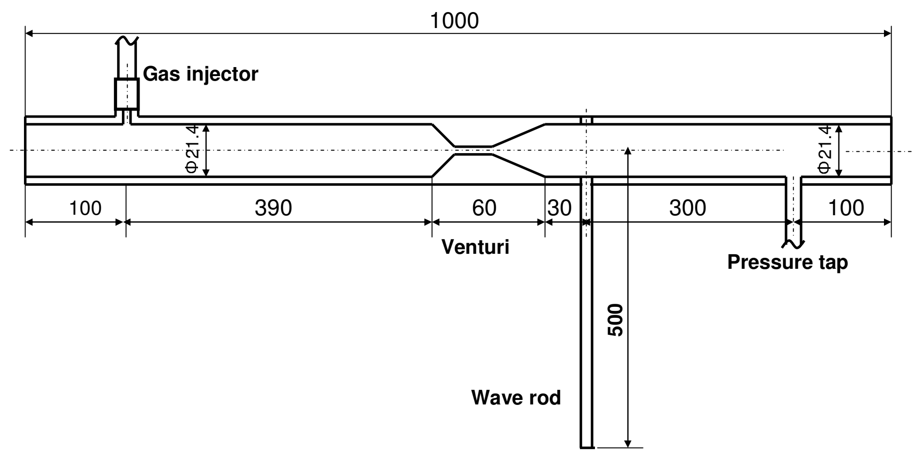

Fig. 2-2. Liquid sodium test section part

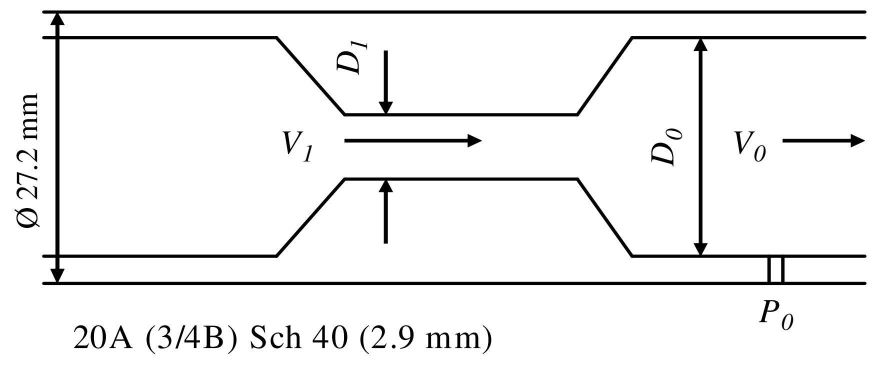

Fig. 2-3. Venturi part of the test section

2.1.2. Water Loop Test Apparatus

The water loop apparatus for cavitation experiment has been constructed at the North Laboratory Building 1 of Research Laboratory for Nuclear Reactors (RLNR), Tokyo Institute of Technology. The loop consists of four main parts, i.e. the pump, the orifice flow rate meter, the acrylic tank and the test section. The pump is a canned motor pump supplied by Teikoku Electric MFG. Co., Ltd. This pump is connected to an inverter to control the rotation speed of the pump. The orifice flow rate meter is used to measure the flow rate of water based on pressure difference between the upstream and downstream of the flow. This orifice flow rate meter is connected with a differential pressure transducer which output signal is proportional with the pressure difference. At the top of the loop, there is a large acrylic tank to contain and circulate water during experiment. Its inner diameter (ID) is 580 mm, outer diameter (OD) is 600 mm and height is 1000 mm. There are three test sections connected to the water loop, i.e. the venturi and entrance nozzle test sections for water cavitation experiments, and the thin film flow test section for thin film flow experiment.

The venturi test section has inner (D_1) and outer diameter (D_0) of 6.5 and 21 mm, respectively. It is made of acrylic resin for observing the cavitation phenomenon that occurs inside of it. The length of the test section part is 200 mm.

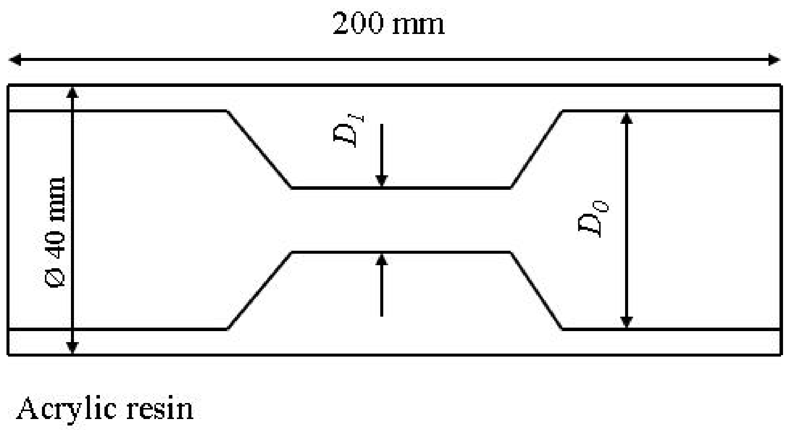

Fig. 2-4. Venturi test section for water cavitation experiment

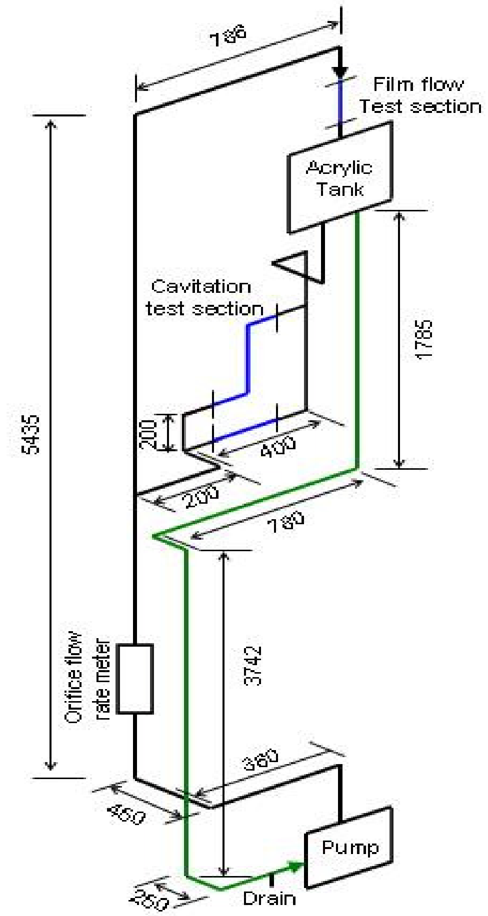

Fig. 2-4. Water loop test apparatus

2.2. Experimental Procedure

2.2.1. Sodium cavitation experiment without argon gas injection

The experiment was conducted at sodium stagnant pressure inside the expansion tank of 0.06-0.18 MPa-a and temperature of 200-400°C. The detailed experimental procedures can be explained as follows:

1) At the beginning, the loop was circulated with a desired level of experimental temperature.
2) The EMP was turned off. Then, the pressure at the expansion tank was controlled to a desired level of experimental conditions by injecting argon gas.
3) When the experimental conditions were all reached, the EMP was turned on again to circulate the liquid sodium.

4) The EMP voltage was increased gradually to the desired cavitation conditions and the experimental data were collected.

2.2.2. Sodium cavitation experiment with argon gas injection

The experiment was conducted at sodium stagnant pressure inside the expansion tank of 0.06~0.18 MPa-a and temperature of 300-400°C. The detailed experimental procedures can be explained as follows:

1) At the beginning, the loop was circulated with a desired level of experimental temperature.
2) The EMP was turned off. Then, the pressure at the expansion tank was controlled to a desired level of experimental conditions by injecting argon gas at the expansion tank.
3) When the experimental conditions were all reached, the EMP was turned on again to circulate the liquid sodium.
4) The desired level of argon gas was injected to the flowing liquid sodium loop, from 0-5 cc/min using a controller through a porous tungsten plug.
5) The EMP voltage was increased gradually to the desired cavitation conditions and the experimental data were collected.

Before the experiment, some components of the sodium loop facility were calibrated first. The components that were calibrated are pressure transducer and electromagnetic flow rate meter (EMF). The pressure transducer (Ashcroft GC-51) was calibrated before the shipment by Nagano Keiki Co., Ltd [16]. The calibration conditions are room temperature (24°C) using nitrogen gas (N_2). The EMF was calibrated at 200°C and 1 atmospheric pressure (1 atm). The results of the calibrated equipments can be seen on Table 2-1 and 2-2.

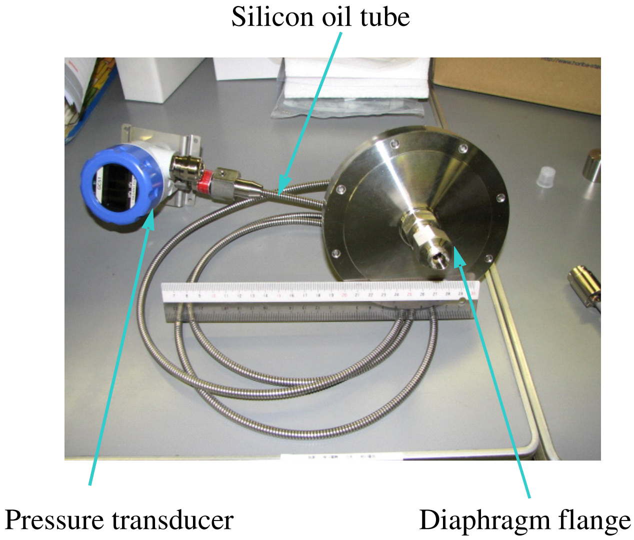

Fig. 2-5. Photograph of diaphragm type pressure gauge

The static pressure of the liquid sodium downstream was sensed by the diaphragm connected at the pressure tap and transmitted along the silicon oil tube to the pressure transducer. This silicon oil tube also acts as a heat resistance to keep the maximum allowable temperature of the pressure gauge below 200°C, as shown in Fig. 2-5.

Table 2-1. Ashcroft GC-51 pressure transducer calibration data

Input (MPa)	**Output (mA DC)**
-0.100	4.00
-0.070	6.40
-0.050	8.00
0.000	12.00
0.050	16.00
1.100	20.00

Table 2-2. EMF calibration data

Output (mV)	Flow rate (L/min)
0.0	6.3
0.8	7.4
1.6	8.7
2.4	10.2
3.2	12.0
4.0	13.9
4.8	16.1
5.6	18.4
6.4	20.9
7.2	23.7
8.0	26.6
8.8	29.8
9.6	33.1
10.0	34.9

Tables 2-3, 2-4 and 2-5 show the characteristic of the pressure transducer, acoustics noise sensor, and the detailed experimental conditions, respectively.

Table 2-3. Pressure transducer characteristics

Specification (pressure gauge)		Specification (diaphragm)	
Pressure range	-0.1-0.1 MPa-g	Diameter	110 mm
Output	4-20 mA	Lower flange material	SUS 316L
Maximum temperature	200°C	Upper flange material	SUS 316

Table 2-4. Sensor characteristics for sodium cavitation

Sensor brand and type	Ono Sokki NP-2710
Sensitivity (pC/m/s²)	0.31±10%
Transverse sensitivity	Within 5%
Capacitance	~340 pF
Frequency response*	fc～10kHz±5% fc～20kHz±3dB
Resonant frequency	~50kHz
Peak operating (m/s^2)	22,600
Shock survivability (m/s^2)	98,000
Operating temperature range (℃)	−70～+260

*fc depends on the time constant of the connected amplifier.

fc = $\frac{1}{2}\pi RC$

Table 2-5. Experimental conditions of the cavitation test

Temperature (°C)	Stagnant Pressure (MPa-absolute)
200	0.06-0.18
300	0.08-0.18
400	0.08-0.18

2.2.3. Water cavitation experiment

The experiment was conducted at water stagnant pressure of 0.06-0.12 MPa-a and water room temperature (10.2-17.6°C). The detailed experimental procedures can be explained as follows:

1) The vacuum pump was turned on to depressurized the system to -30 cmHg.
2) The motor pump to circulate water in the loop was turned on and the speed was increased gradually until cavitation occurred in the venturi region.

3) The downstream pressure, water flow rate, water temperature, and spectrum are recorded by using CADAC-21 and visual analyzer. Accelerometer TEAC 601 is used to measure the cavitation noise signal
4) The cavitation phenomenon in venturi was recorded by using a high-speed camera system connected to a computer.
5) The above procedures were repeated again with different stagnant pressure conditions, i.e. -10 cmHg, 0.1 kgf/cm^2 and 0.2 kgf/cm^2. No cavitation found at 0.36 kgf/cm^2 (atmospheric pressure condition).

Table 2-6. Calibration data of orifice flow rate meter

Pressure difference (%)	Flow rate^2 [(l/min)^2]
0	0
23	208.6
24	242.2
33	332.3
38	359.1
46	517.3
49	528.3
50	513.6
64	672.0
67	655.9
87	1002.5
90	940.2
92	861.8
98	1073.5
101	975.7
$y = 1040.9x - 6.1218$	

The orifice flow rate meter connected with the differential pressure transducer for measuring the flow rate was calibrated first before the experiment. The calibration was conducted by measuring the change of the water level inside the water tank and counting the time change using a stopwatch. The calibration was performed at water temperature of 10°C, orifice diameter of 10 mm and atmospheric condition (1 atm). The calibration data can be seen in Table 2-6 above. Table 2-7 shows the sensor characteristics for water cavitation.

Table 2-7. Sensor characteristics for water cavitation

Sensor brand and type	TEAC 601
Sensitivity ($pC/m/s^2$)	0.3±20%
Transverse sensitivity	5%
Capacitance	1,000±20% pF
Frequency response*	fc～30,000 Hz
Resonant frequency	~60kHz
Peak operating (m/s2)	±100,000
Shock survivability (m/s2)	200,000
Operating temperature range (℃)	−20～+80

CHAPTER III

Acoustic Noise and Onset of Sodium Cavitation in Venturi without Argon Gas Injection

3.1. Introduction

Sodium-cooled fast reactor (SFR) is one of the proposed future nuclear reactors known as Generation IV nuclear reactors. It is fast spectrum reactor using a closed fuel cycle with full actinide recycle. Its main missions are to reduce the physical demand on repositories, and utilize the entire natural resource for fissionable materials. SFRs are the most technologically developed of the six Gen-IV systems. SFRs have been built and operated in France, Japan, Germany, the U.K., Russia or the U.S.S.R., and the U.S. There are some demonstration plants already built ranged from 1.1 MWth (at EBR-I in 1951) to 1200 MWe (at SuperPhenix in 1985), and some other sodium-cooled reactors today in Japan, France, and Russia [17-19]. The deployment date for sodium-cooled fast reactor is estimated around 2020 [6].

One of the key issues in fluid-dynamic design of the sodium-cooled fast reactors is inhibition of cavitation and/or its influence. Cavitation can be regarded as an ebullition process that takes place if the bubble grows explosively in an unbounded manner as liquid rapidly changes into vapor. This situation occurs when the pressure level goes below the vapor pressure of the liquid [20]. Brennen [21] regarded the cavitation phenomenon as a decrease in the tensile strength of the liquid similar to that in the solid, and the decrease is considered long enough to create bubbles. The phenomenon of cavitation itself can have some influences. The influences could be classified into fluid-dynamic, mechanical, and core neutronics performances as follows: the occurrence of cavitation affects fluid-dynamic performances of flow regulating mechanisms in inner structure of reactor vessel; the collapse of cavitation bubbles produces shock waves that damage the edges of orifices, which changes flow rate distribution in core; the shock waves also damage structural material and piping walls; vibrations due to cavitation cause metal fatigue of piping systems; and the entry of cavitation bubbles into core causes instability of core reactivity. Cost-down effort in design leads to more compact reactor vessel and components, which makes the cavitation to occur readily because of higher coolant velocity in coolant flow circuits. According to Kale *et al.* [22], the damage of the structural parts in the vicinity of the cavitating zone and its severity is found to be 1.5 to 2 times more severe compared to that in water, and also the cavitation phenomenon could lead to the overheating of the fuel clad due to the vapor cavities produced when enter to the fuel passages.

Furthermore, most of the experimental studies for investigating the sodium cavitation phenomenon in designing the sodium-cooled fast reactors were conducted using water as simulant fluid. Therefore, there are scarcities of data for sodium cavitation nowadays. These lacks of data could be a major obstacle in evaluating the onset of cavitation and its influence in sodium-cooled fast reactor. The present study is intended to understand the phenomenon of cavitation in liquid sodium as well as its acoustic noise characteristics.

3.2. Result and Discussion

The results of the experiments are presented in Fig. 3-1 to 3-14. Fig. 3-1 and 3-2 show the result of the noise intensity over cavitation coefficient *K* at 300 and 400°C. The results show that the noise intensity is relatively low when there is no cavitation in the venturi region (*K* is higher than unity). The noise intensity begins to rise rapidly when *K* approaches unity (onset of cavitation). Under developed cavitation condition (*K* is lower than unity), the noise intensity is relatively stable without changing dramatically. The stagnant pressure at the expansion tank has no effect on the noise intensity in developed cavitation conditions. The noise intensity at 400°C has no significant differences with that at 300°C, which is around 43 dB RMS. The onset of cavitation was determined by hearing the sound of the cavitation test section and checking the spectrum analyzer monitor. It was concluded that cavitation occurred (onset of cavitation) when there was a rise in the amplitude of the spectrum analyzer, and rapid knocking sounds in the test tube. The determination of the onset condition is rather subjective since sodium is opaque.

The cavitation coefficient *K* in this experiment is derived from the Bernoulli`s equation for incompressible flow.

$$P_1 + \frac{\rho}{2} V_1^2 = P_0 + \frac{\rho}{2} V_0^2 \qquad (2)$$

where P_1 is the static pressure at venturi, ρ is the liquid sodium density at given temperature, V_1 is the liquid sodium velocity at venturi region, P_0 is the static pressure at downstream, and V_0 is the liquid sodium velocity at downstream region. If P_1 is close to the saturation pressure P_v of the liquid sodium, then the cavitation coefficient K can be expressed as

$$K = \frac{P_0 - P_V}{\frac{\rho}{2}\left(V_1^2 - V_0^2\right)} \tag{3}$$

and for $V_1 >> V_0$

$$K \approx \frac{P_0 - P_V}{\frac{\rho}{2} V_1^2} \tag{4}$$

where P_v is the sodium saturation pressure at given temperature. According to the theory, cavitation starts to occur when cavitation coefficient K is equal to unity. From the data obtained, it is clear that cavitation coefficient K can be used as a raw prediction of the onset cavitation conditions.

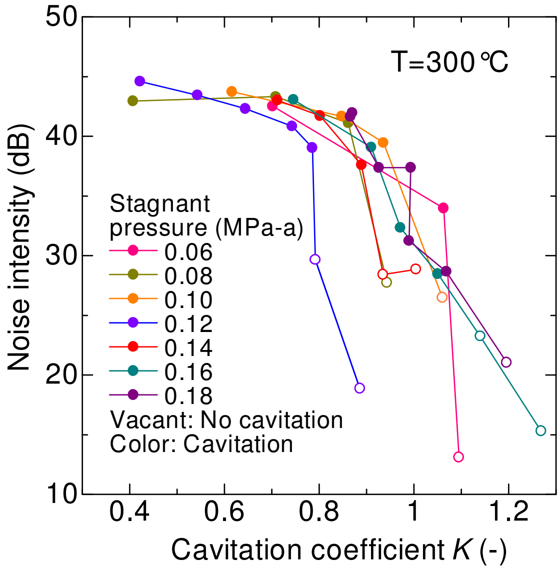

Fig. 3-1. Noise intensity as a function of cavitation coefficient at 300°C

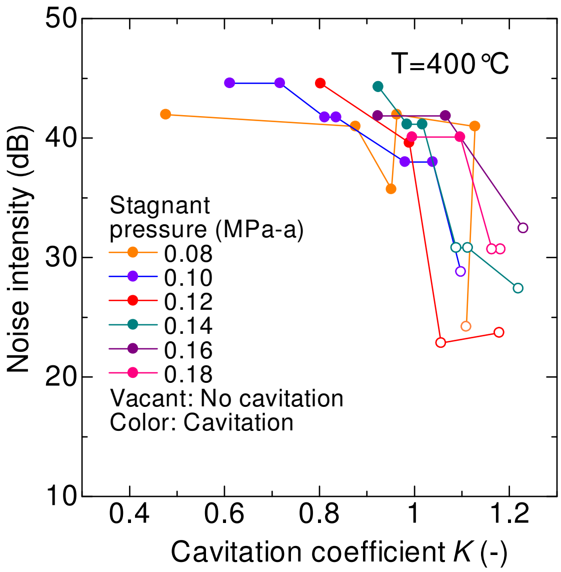

Fig. 3-2. Noise intensity as a function of cavitation coefficient at 400°C

Figs. 3-3, 3-4 and 3-5 show the results of no cavitation and occurrence of cavitation on the map of the venturi velocity as a function of cavitation coefficient at 200, 300 and 400°C, respectively. For every temperature rise, it is apparent that the stagnant pressure in the expansion tank has influence on the onset cavitation velocity in the venturi. The velocity in the venturi increases with the increase of the stagnant pressure conditions. The velocity becomes relatively stable in the developed cavitation conditions. Cavitation coefficient at the onset of cavitation was nearly equal to unity. However, an increase in temperature shifted the cavitation coefficient to a value a little higher than unity. From these figures it can be concluded that the formation of the cavitation bubbles is suppressed at higher stagnant pressure, therefore the onset cavitation velocity in the venturi increases. It is noted also from the figures that there are two distinct regions, the no cavitation region (K>1), and the cavitation region (K<1).

These figures also show that if the cavitation coefficient below the value of unity, the cavitation velocity in the venturi is relatively constant. This is similar to the phenomenon of the critical or the choked flow. In the critical or choked flow phenomenon, the decrease in the downstream pressure below a certain level of critical pressure does not significantly increase the flow rate. For cavitation in a venturi, the critical flow phenomenon might be caused by the decrease of the sound velocity in the liquid sodium due to the formation of cavitation bubbles or by the carried under cavitation bubbles into the EMP that decreases the pump performance.

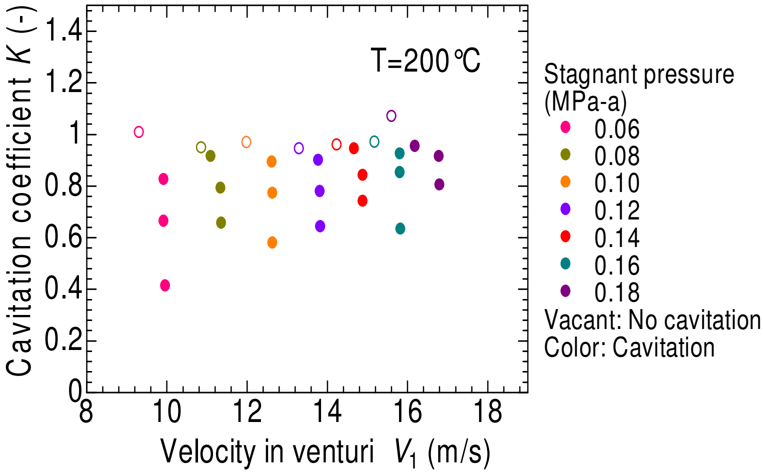

Fig. 3-3. Cavitation coefficient K as a function of venturi velocity at 200°C

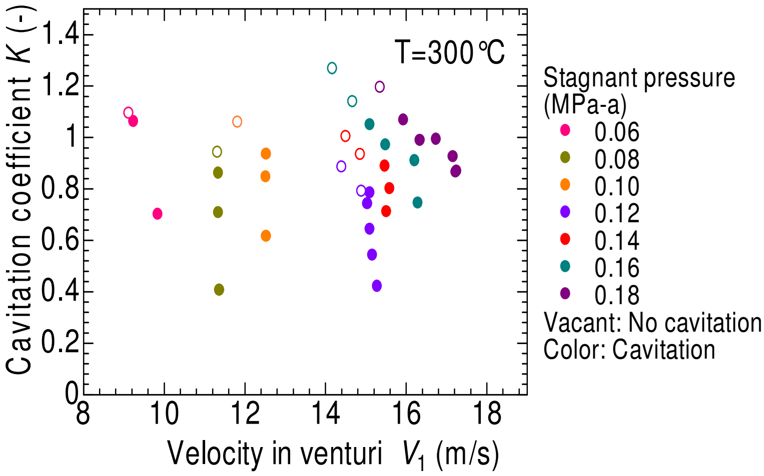

Fig. 3-4. Cavitation coefficient K as a function of venturi velocity at 300°C

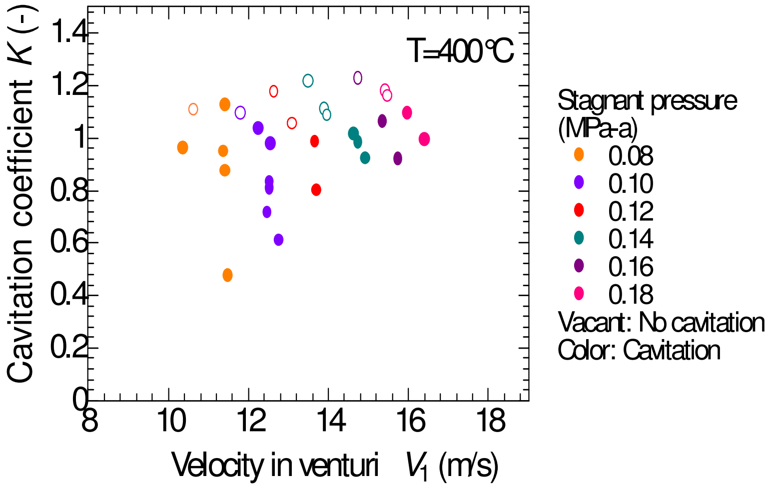

Fig. 3-5. Cavitation coefficient *K* as a function of venturi velocity at 400°C

Fig. 3-6 shows the resonance frequency of the test section at 200°C and 0.12 MPa absolute (MPa-a). This figure was obtained from hitting the test section by hammer several times when the electromagnetic pump was turned off. The resonance frequencies of the test section are indicated by the peaks of noise intensity around 1000, 3000, 5000, 9000, and 20,000 Hz as shown in Fig. 3-6. The noise intensities have the significant increase in the high frequency region than in the low frequency region.

Figs. 3-7 to 3-10 show the results of the noise intensity over frequency at different temperature and stagnant pressure conditions at 200°C. The results show that an increase in noise intensity is significant at higher frequencies (above 10,000 Hz) than at lower ones. During the no cavitation conditions, the noise intensity at the higher frequencies is relatively lower compared to that at the lower ones. When cavitation starts to occur (intermittent cavitation), the noise intensity at the higher frequencies starts to increase more than at the lower ones. At developed cavitation conditions, the noise intensity at the higher frequencies is almost similar to that at the lower ones. This indicates that there are no significance differences in the magnitude of the noise intensity over the entire frequencies spectrum when cavitation is in the developed conditions. The change of the stagnant pressure in the expansion tank from 0.08 to 0.18 has no effect on the magnitude of the noise intensity. It can be concluded that the magnitude of cavitation noise intensity at 200°C is independent of the stagnant pressure changing. These figures also show some resonance peaks similar with those obtained in Fig. 3-6.

Figs. 3-11 and 3-13 show the results at 300°C. The results at 300°C are almost similar with those at 200°C, except at 0.14 and 0.18 MPa-a. At 0.08 MPa-a, the increase of the noise intensity at lower frequencies are lower than that at higher frequencies. While at 0.14 and 0.18 MPa-a, the cavitation noise intensity increases both at lower and high frequency regions. Therefore, at 0.14 and 0.18 MPa-a the noise intensity of no cavitation and developed cavitation conditions can be distinguished clearly by observing the magnitude change of the noise intensity at low and high frequency regions. The similar resonance peaks can also be seen clearly at 300°C as in 200°C.

At 400°C and different stagnant pressure in the expansion tank (Figs. 3-14 to 3-16), there are clear distinctions on the noise intensities at no cavitation and cavitation conditions. When there is no cavitation, the magnitude of the noise intensity is relatively low (around -70 dB) both at low and high frequency regions. If cavitation starts to occur in the venturi, the noise intensity starts to increase to a higher value (around -45 dB), both in low and high frequency regions.

For 400°C, the noise intensity becomes unstable. It means that sometimes the magnitude of the noise intensity was large (similar to the noise generated by the developed cavitation conditions) for a relatively long time, but then the noise became relatively low (similar to the noise generated by the no cavitation conditions). These instabilities of the noise intensities were probably caused by the increasing amount of cavitation bubbles due to the higher vapor pressure. Further examinations are needed to understand the cause of these instabilities at high temperature (400°C).

From the data obtained at 200, 300, and 400°C, it can be concluded that the stagnant pressure change at the expansion tank does not affect the magnitude of the noise intensity at 200, 300, and 400°C. Therefore, it is independent of the stagnant pressure level.

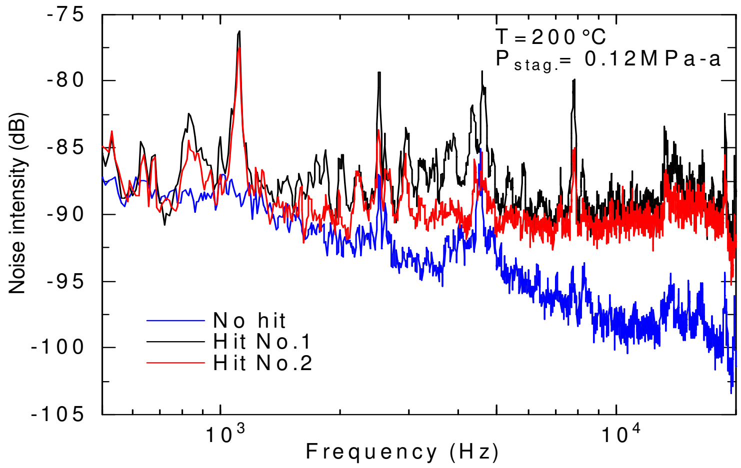

Fig. 3-6. Resonance frequency of the test section

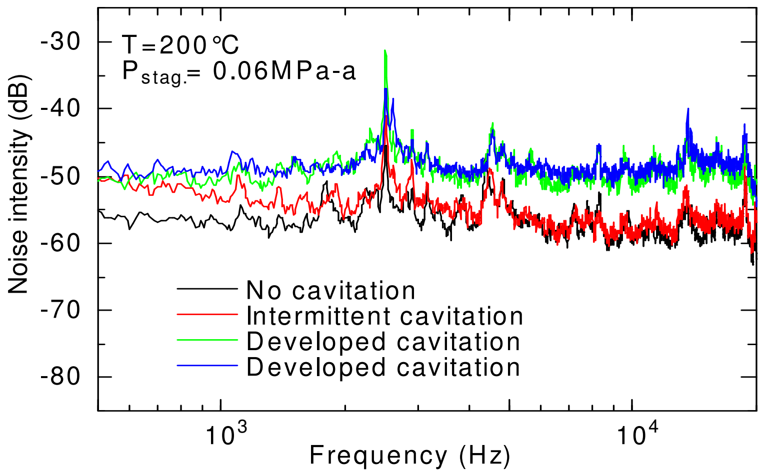

Fig. 3-7. Noise intensity as a function of frequency at 200°C and 0.06 MPa-a

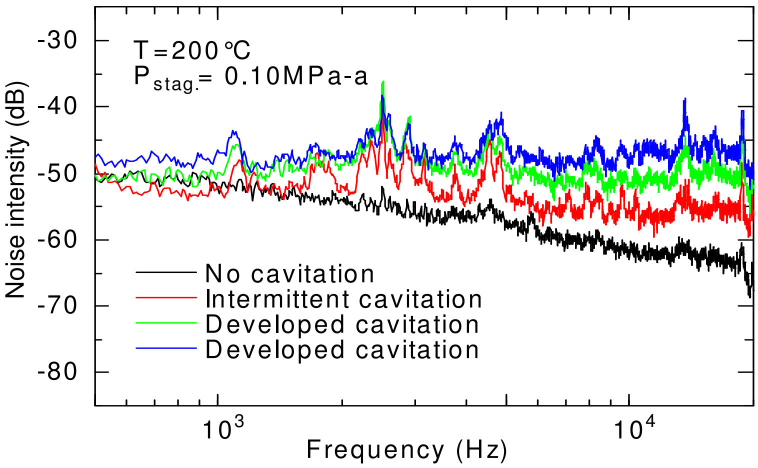

Fig. 3-8. Noise intensity as a function of frequency at 200°C and 0.10 MPa-a

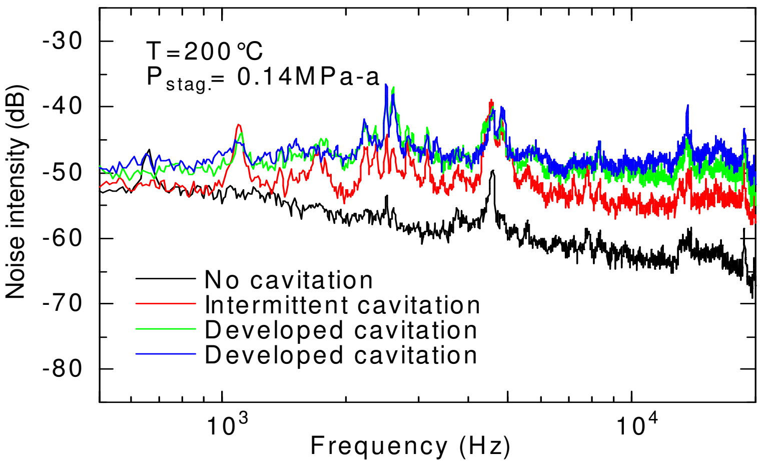

Fig. 3-9. Noise intensity as a function of frequency at 200°C and 0.14 MPa-a

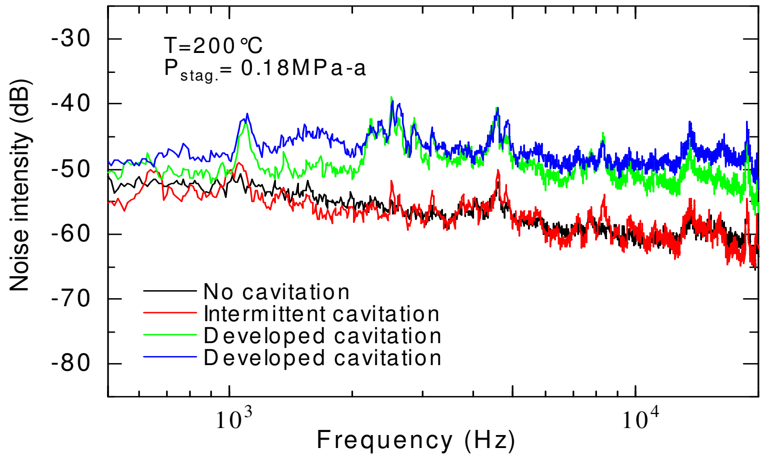

Fig. 3-10. Noise intensity as a function of frequency at 200°C and 0.18 MPa-a

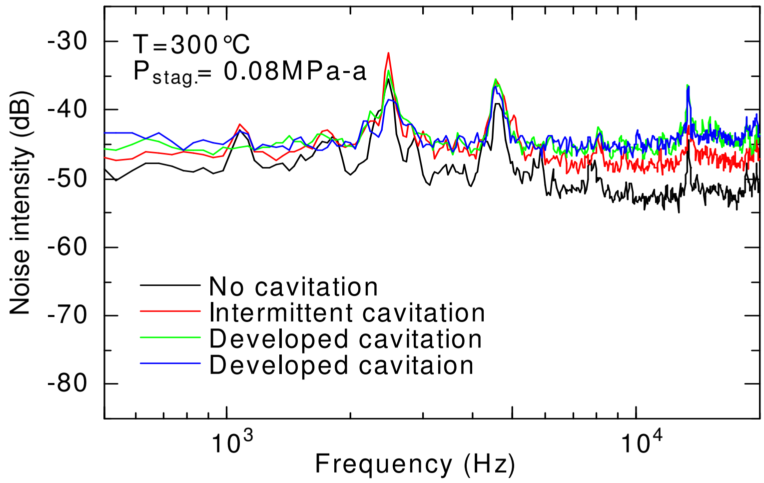

Fig. 3-11. Noise intensity as a function of frequency at 300°C and 0.08 MPa-a

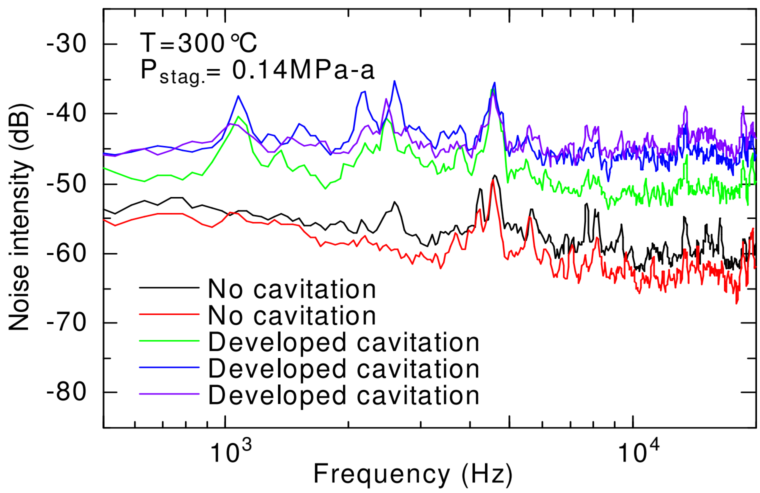

Fig. 3-12. Noise intensity as a function of frequency at 300°C and 0.14 MPa-a

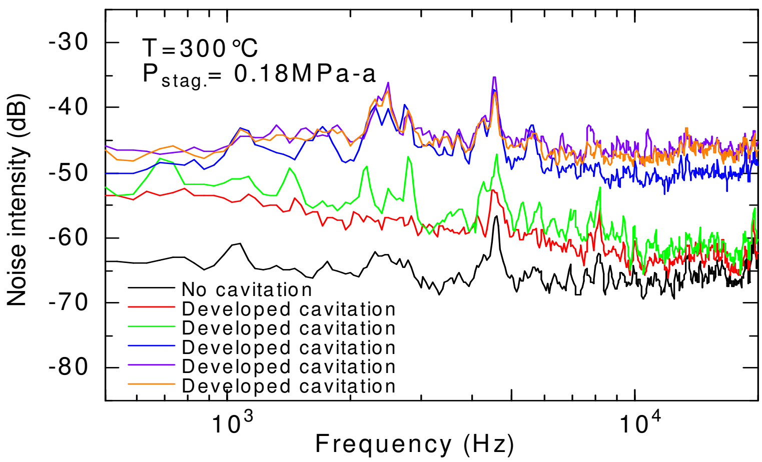

Fig. 3-13. Noise intensity as a function of frequency at 300°C and 0.18 MPa-a

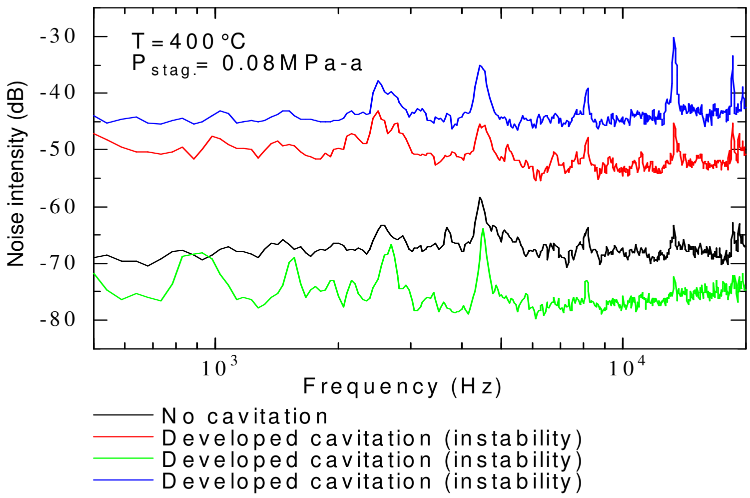

Fig. 3-14. Noise intensity as a function of frequency at 400°C and 0.08 MPa-a

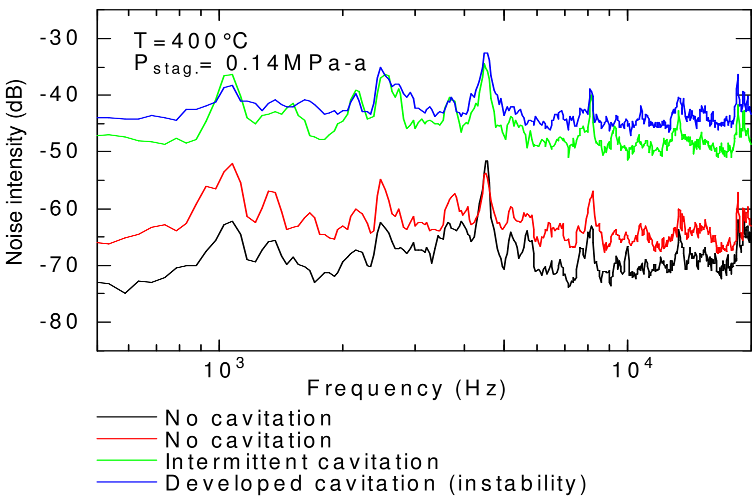

Fig. 3-15. Noise intensity as a function of frequency at 400°C and 0.14 MPa-a

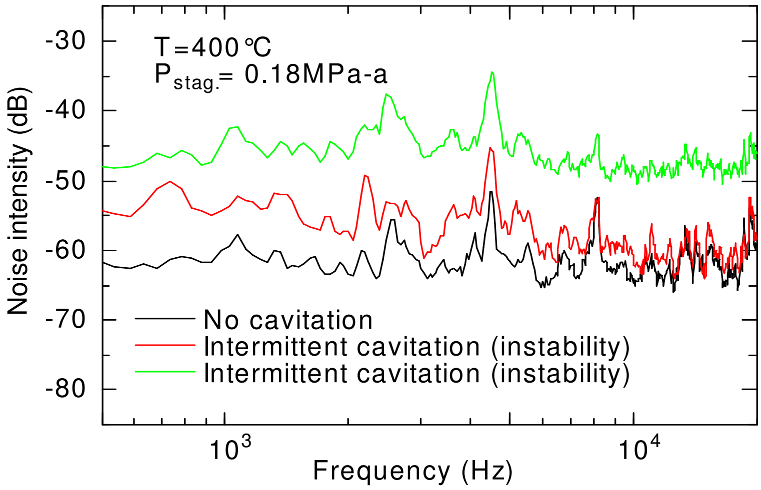

Fig. 3-16. Noise intensity as a function of frequency at 400°C and 0.18 MPa-a

3.3. Conclusion

Sodium cavitation inception conditions were clarified for a venturi. The test section is a venturi with 6.5 mm in inner diameter and 20 mm in length. The experiments were conducted at sodium stagnant pressure in the expansion tank of 0.06-0.18 MPa and temperature of 200-400°C. The following conclusions have been reached from the experimental results:

1) The noise intensity starts to increase dramatically when cavitation occurs inside the test section.
2) The stagnant pressure at the expansion tank has no effect in the magnitude of the cavitation noise intensity.
3) The stagnant pressure at the expansion tank has clear effect on the onset cavitation velocity in the venturi. The higher the stagnant pressure, the faster the velocity in the venturi to initiate cavitation.
4) At 200°C, an increase in the noise intensity is larger at higher frequencies than at lower ones in intermittent cavitation conditions, and the magnitude becomes relatively similar between low and high frequency regions in developed cavitation conditions.
5) At 300°C and lower stagnant pressure condition, the increase of the noise intensity in developed cavitation conditions is similar to that as in 200°C. While at higher stagnant pressure conditions, the increase can be seen both in low and

high frequency regions.

6) At 400°C and no cavitations, the noise intensity is relatively low both in low and high frequency regions. When cavitation starts to occur, the noise intensity increases both in low and high frequency regions.
7) Instability conditions occur at high temperature condition (400°C) in the sodium loop. It may be caused by the increasing amount of cavitation bubbles due to the higher vapor pressure. Further examinations are needed to understand the cause of these instabilities at high temperature.

From this experiment it is recommended to conduct another cavitation research with different parameters to give a better understanding in the liquid sodium cavitation phenomenon.

CHAPTER IV

Acoustic Noise and Onset of Sodium Cavitation in Venturi with Argon Gas Injection

4.1. Introduction

The existence of the free surface in the vessel of the sodium-cooled fast reactor is to accommodate the expansion and to prevent the ingress of air from the atmosphere and contact with the hot liquid sodium. Since sodium-cooled fast reactor has higher volumetric power density, the high flow rate must be maintained to control the temperature of the core. In this condition, entrainment of argon gas from the free surface to the other parts of the reactor systems, such as intermediate heat exchanger (IHX), pumps and coolant channel, is possible [23, 24]. The entrainment could occur with different mechanism such as surface vortices etc. This entrainment could result in unfavorable operational conditions such as reduce the heat transfer of liquid sodium in the IHX parts, cavitations in pumps or in coolant channels, and difficulties in controlling the steady flow rate conditions over the entire operational conditions.

In the case of cavitation phenomenon, the effect of argon gas injection in the fluid could dissolve the gas and enhance the formation of cavitation bubbles. Therefore, cavitation could start preliminary than expected [21]. The present experiment was conducted to understand the phenomena of cavitation with the influence of argon gas injection to simulate the entrainment of argon cover gas in the flowing liquid sodium coolant.

4.2. Result and Discussion

The results of the cavitation experiment in liquid sodium with the injection of argon gas are shown in Fig. 4-1. to 4-50. Fig. 4-1 to 4-4 show the results of the noise intensity as a function of cavitation coefficient with argon gas injection from 0-5 cc/min at liquid sodium temperature of 300°C. From the results, it can be clearly seen that there are two different regions, the non-cavitation region (marked with vacant symbol) and cavitation region (marked with solid color symbol). Cavitation starts to occur when cavitation coefficient is approximately unity. When there is no cavitation occurred in the loop, the noise intensity is relatively low (below 40 dB RMS). The occurance of cavitation creates an increase in the noise intensity above 40 dB RMS. In the developed-cavitation region (indicated by the decrease of the cavitation coefficient below unity), the noise intensity is relatively constant (around 50 dB) for every stagnant pressure and flow rate of the injected argon gas. The figures show that the noise intensity is relatively similar despite the fact that the stagnant pressure and the flow rate of the injected argon gas are different.

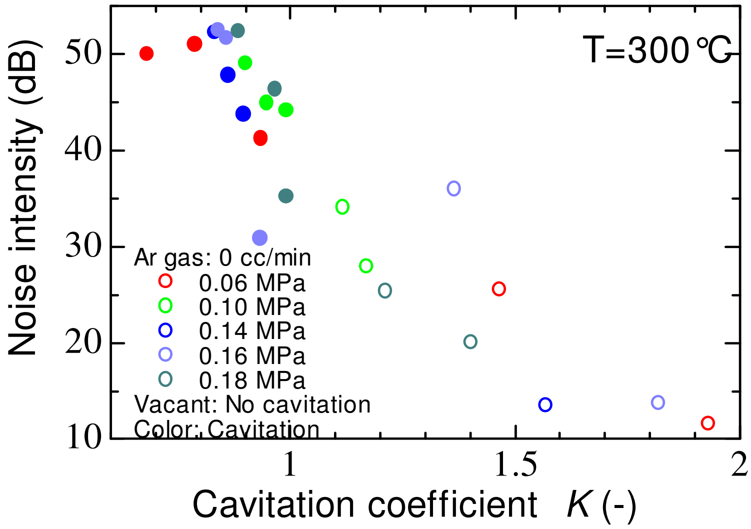

Fig. 4-1. Noise intensity as a function of cavitation coefficient at 300°C (Ar: 0 cc/min)

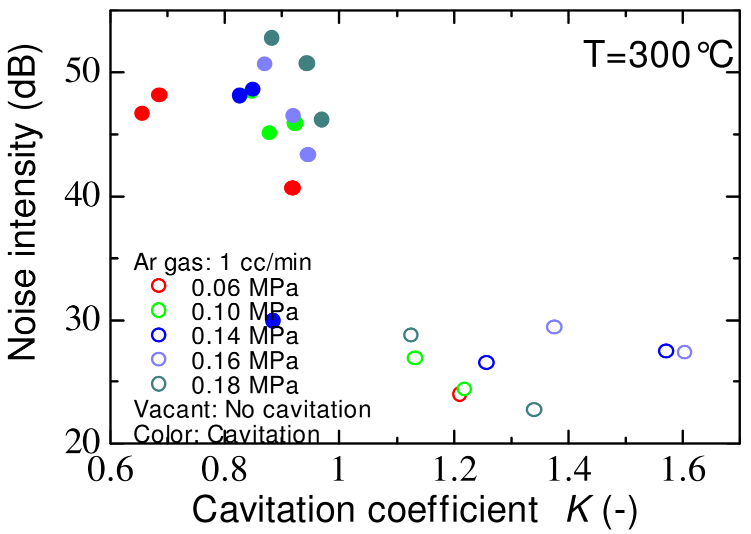

Fig. 4-2. Noise intensity as a function of cavitation coefficient at 300°C (Ar: 1 cc/min)

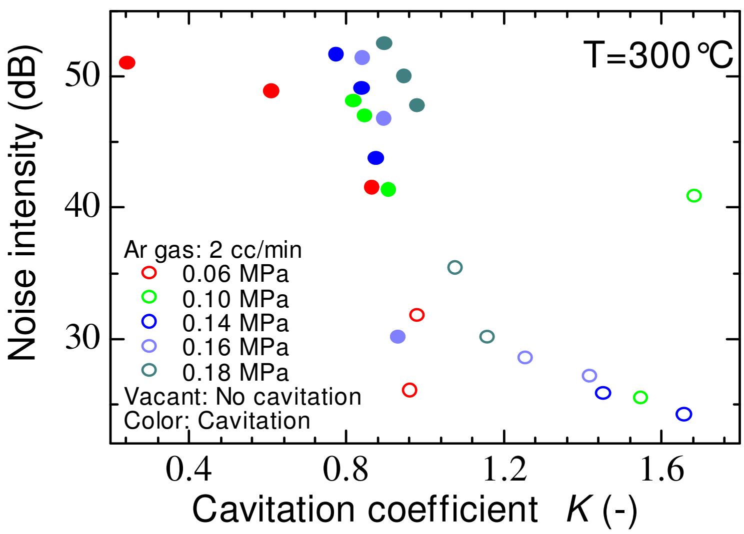

Fig. 4-3. Noise intensity as a function of cavitation coefficient at 300°C (Ar: 2 cc/min)

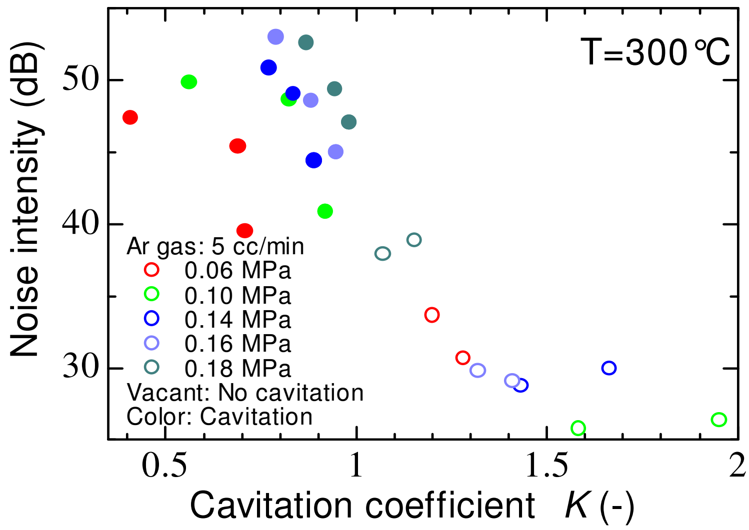

Fig. 4-4. Noise intensity as a function of cavitation coefficient at 300°C (Ar: 5 cc/min)

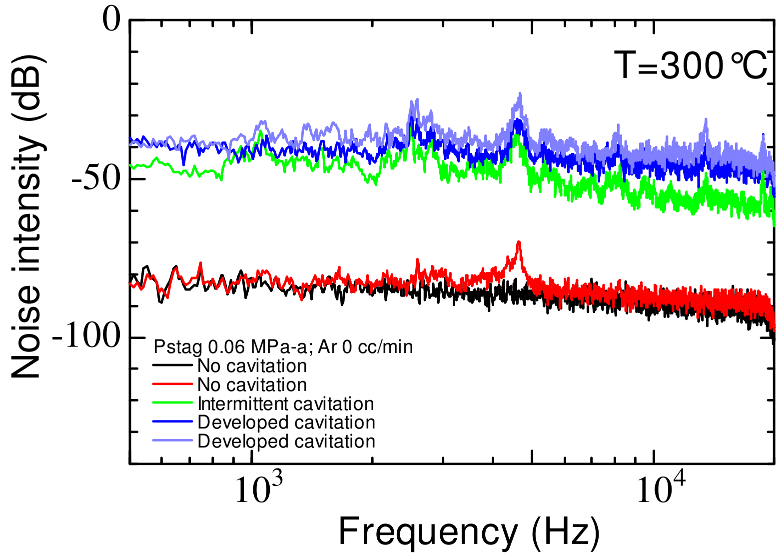

Fig. 4-5. Noise intensity as a function of frequency at 300°C (Pstag: 0.06 MPa-a, Ar: 0 cc/min)

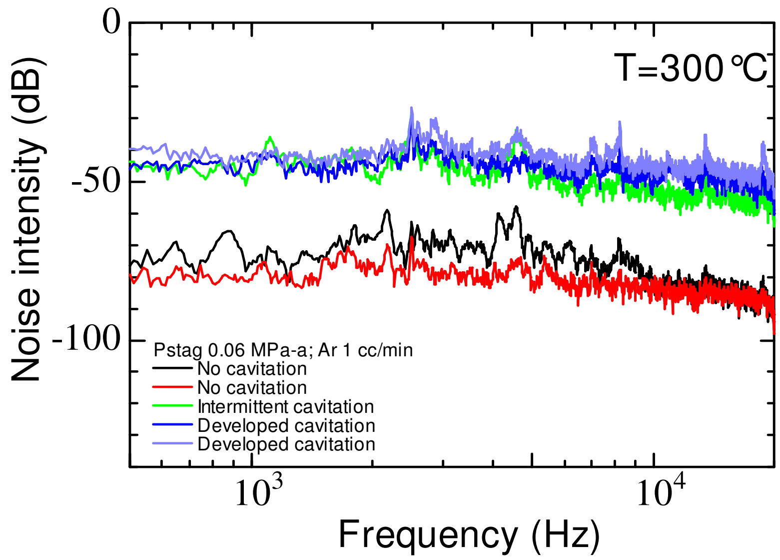

Fig. 4-6. Noise intensity as a function of frequency at 300°C (Pstag: 0.06 MPa-a, Ar: 1 cc/min)

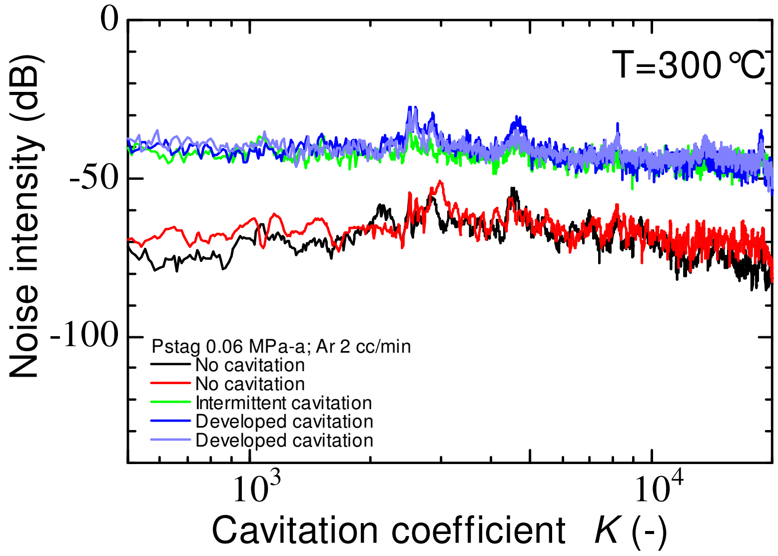

Fig. 4-7. Noise intensity as a function of frequency at 300°C
(Pstag: 0.06 MPa-a, Ar: 2 cc/min)

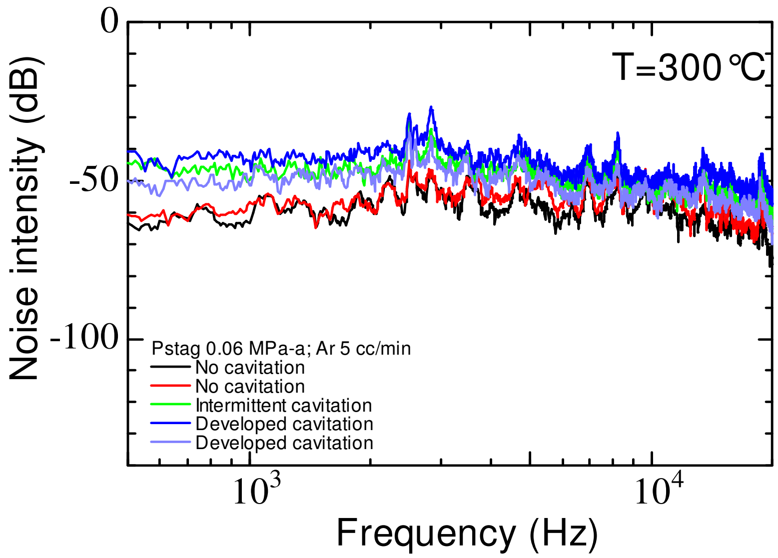

Fig. 4-8. Noise intensity as a function of frequency at 300°C
(Pstag: 0.06 MPa-a, Ar: 5 cc/min)

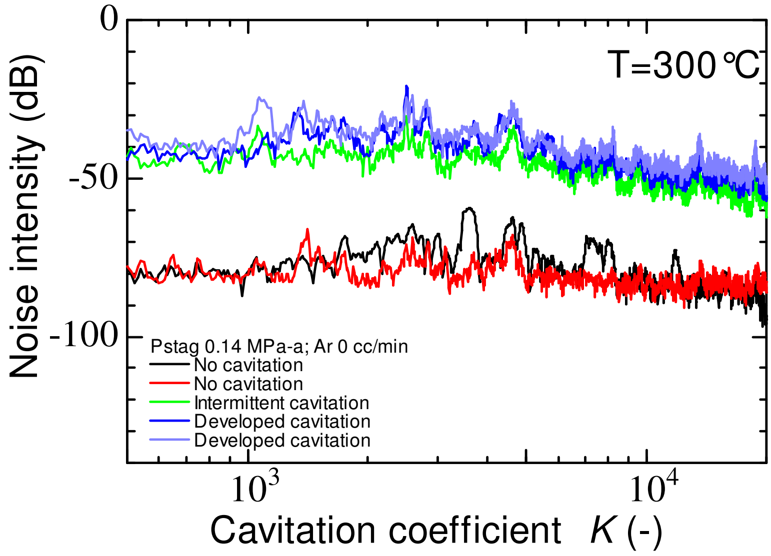

Fig. 4-9. Noise intensity as a function of frequency at 300°C

(Pstag: 0.14 MPa-a, Ar: 0 cc/min)

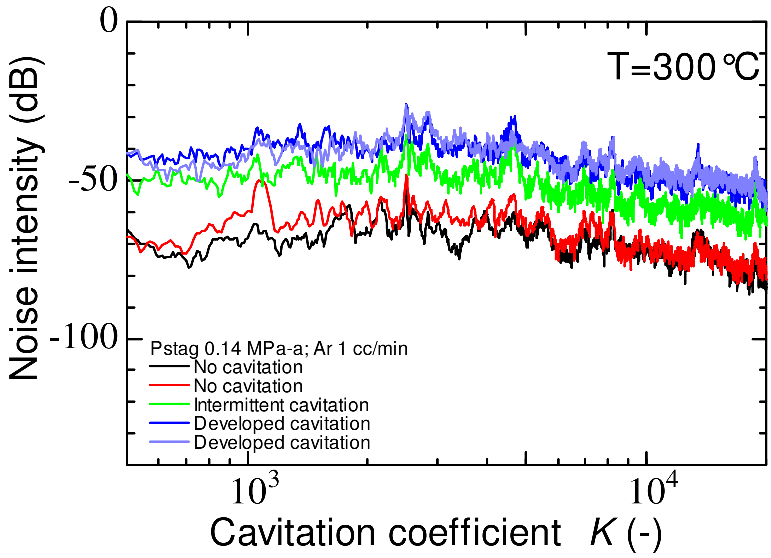

Fig. 4-10. Noise intensity as a function of frequency at 300°C

(Pstag: 0.14 MPa-a, Ar: 1 cc/min)

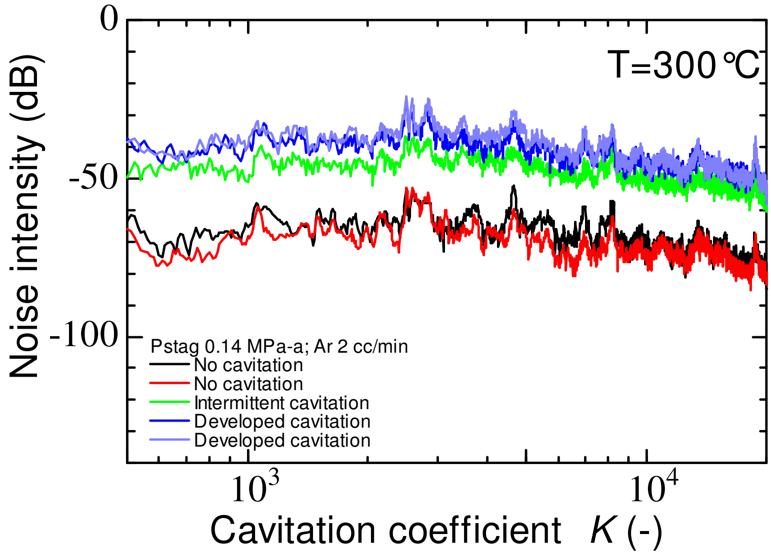

Fig. 4-11. Noise intensity as a function of frequency at 300°C
(Pstag: 0.14 MPa-a, Ar: 2 cc/min)

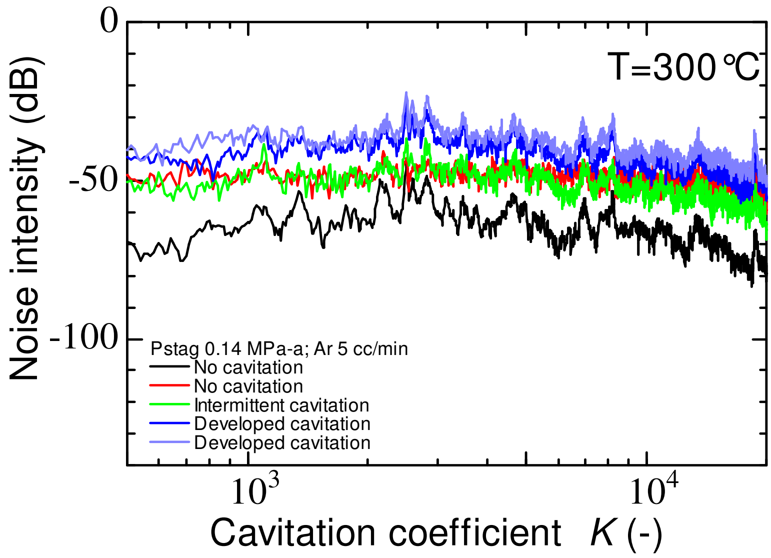

Fig. 4-12. Noise intensity as a function of frequency at 300°C
(Pstag: 0.14 MPa-a, Ar: 5 cc/min)

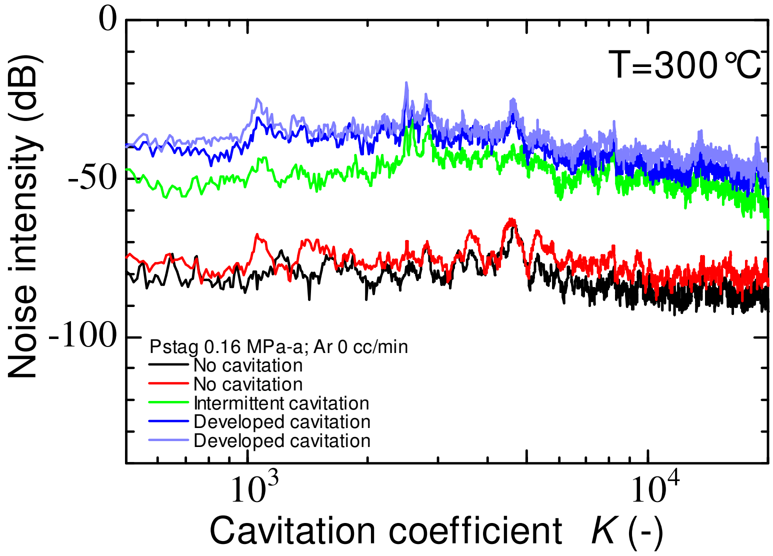

Fig. 4-13. Noise intensity as a function of frequency at 300°C
(Pstag: 0.16 MPa-a, Ar: 0 cc/min)

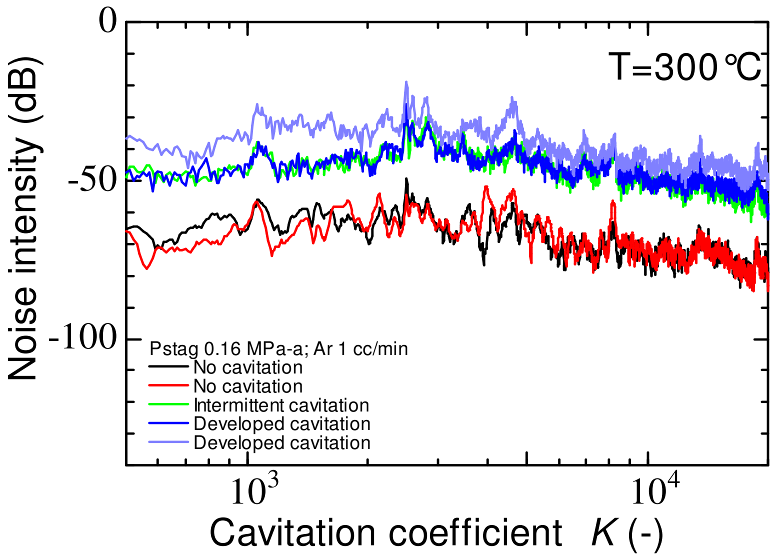

Fig. 4-14. Noise intensity as a function of frequency at 300°C
(Pstag: 0.16 MPa-a, Ar: 1 cc/min)

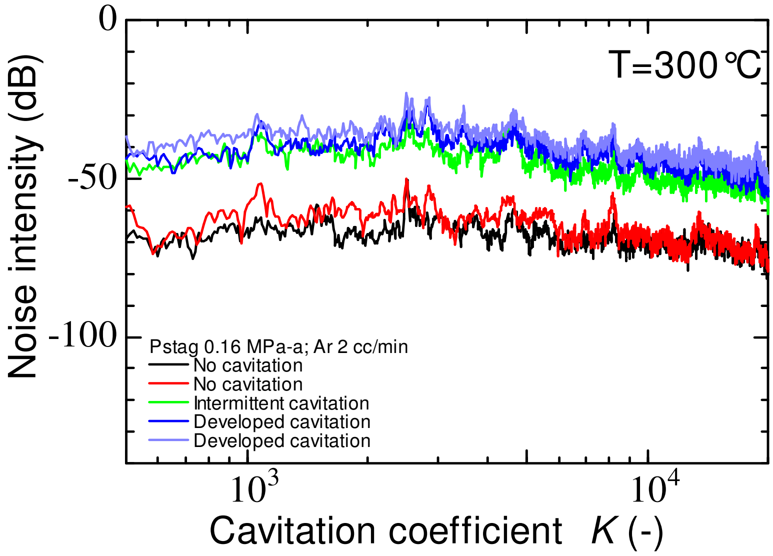

Fig. 4-15. Noise intensity as a function of frequency at 300°C
(Pstag: 0.16 MPa-a, Ar: 2 cc/min)

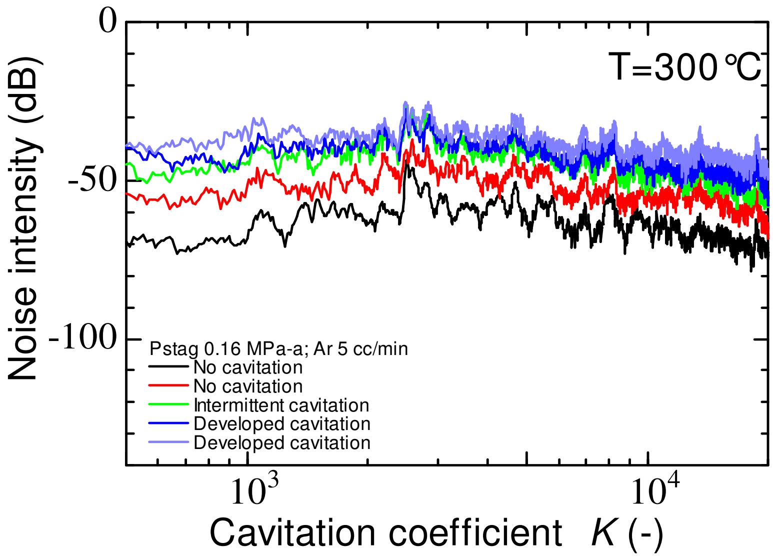

Fig. 4-16. Noise intensity as a function of frequency at 300°C
(Pstag: 0.16 MPa-a, Ar: 5 cc/min)

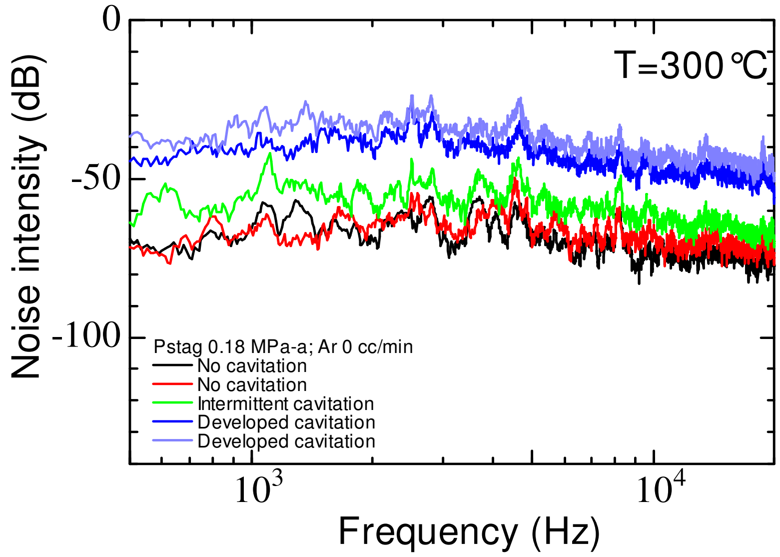

Fig. 4-17. Noise intensity as a function of frequency at 300°C
(Pstag: 0.18 MPa-a, Ar: 0 cc/min)

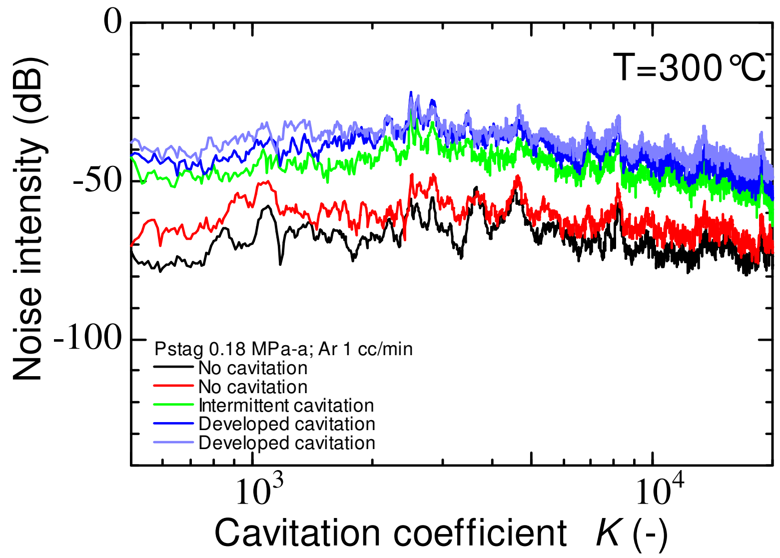

Fig. 4-18. Noise intensity as a function of frequency at 300°C
(Pstag: 0.18 MPa-a, Ar: 1 cc/min)

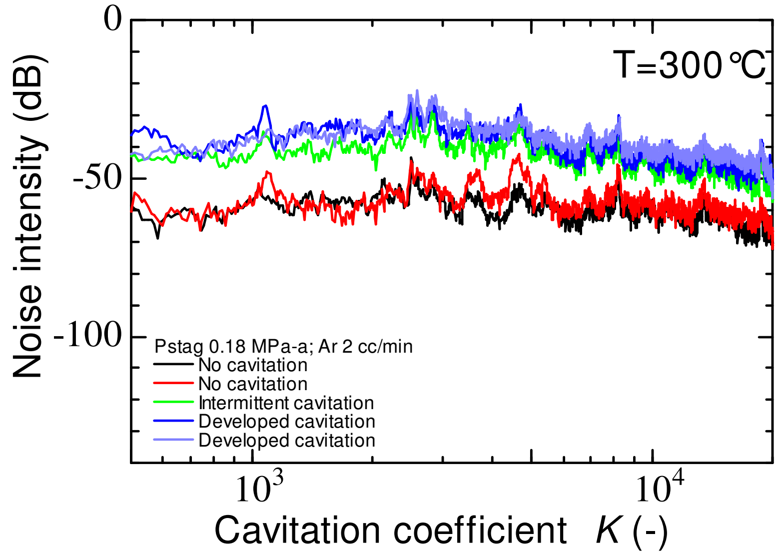

Fig. 4-19. Noise intensity as a function of frequency at 300°C
(Pstag: 0.18 MPa-a, Ar: 2 cc/min)

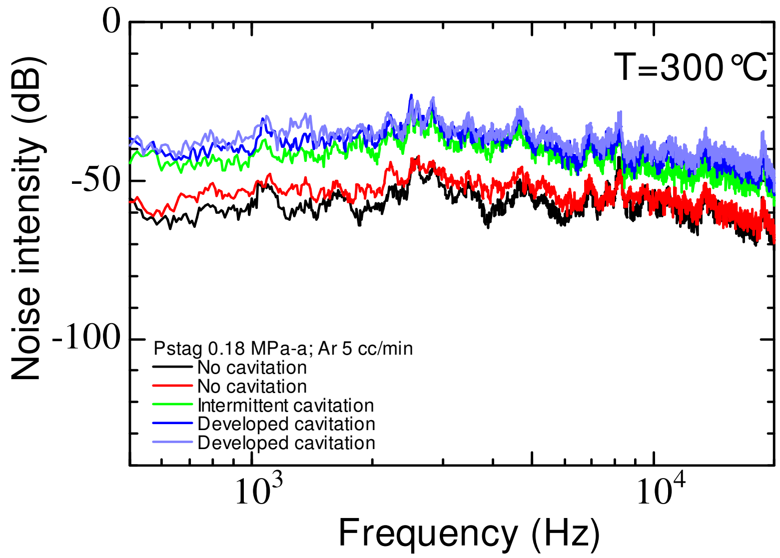

Fig. 4-20. Noise intensity as a function of frequency at 300°C
(Pstag: 0.18 MPa-a, Ar: 5 cc/min)

Fig. 4-5 to 4-20 show the results of the noise intensity as a function of frequency for different expansion tank stagnant pressure and argon gas injection flow rate at

300°C. The frequency data taken for the experiment ranging from 0-20,000 Hz. The results show similar phenomena at non-cavitation, intermittent-cavitation and developed-cavitation conditions. At non-cavitation condition, the noise intensity is relatively flat over the entire frequency range (0-20,000 Hz), i.e. around -70 to -80 dB. The noise intensity begins to rise at intermittent-cavitation condition and becomes constants at developed-cavitation condition, i.e. around -40 dB. The noise intensity at developed-cavitation condition is flat also, similar with that obtained at non-cavitation condition. The effect of the argon gas injection and stagnant pressure has no distinguish effect on the noise intensity produced by cavitation bubbles collapse.

Fig. 4-21 to 4-24 show the result of sodium superficial velocity in venturi as a function of liquid sodium static downstream pressure at 300°C and expansion tank stagnant pressure from 0.06-0.18 MPa-a. It can be clearly seen from the figures that the different stagnant pressure condition has a clear effect on the liquid sodium superficial velocity in the venturi. The higher the stagnant pressure at the expansion tank increase the liquid sodium superficial velocity from around 10 m/s at 0.06 MPa-a to around 16.5 m/s at 0.18 MPa-a. The figures show that there is a saturated velocity when the static downstream pressure decreased during cavitation. These phenomena are similar with the choked/critical flow phenomena and the results are similar with those obtained in the previous Chapter III. The increase of the voltage of the EMP does not increase the liquid sodium superficial velocity. The injection of argon gas into the flowing liquid sodium loop does not change the superficial velocity of liquid sodium. Clearly it has no significant effect at the saturation condition.

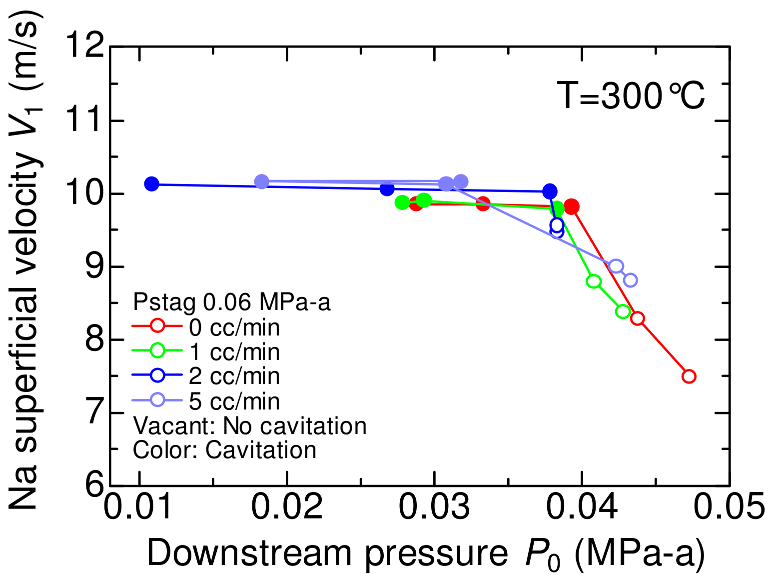

Fig. 4-21. Na superficial velocity as a function of downstream pressure at 300°C (Pstag: 0.06 MPa-a)

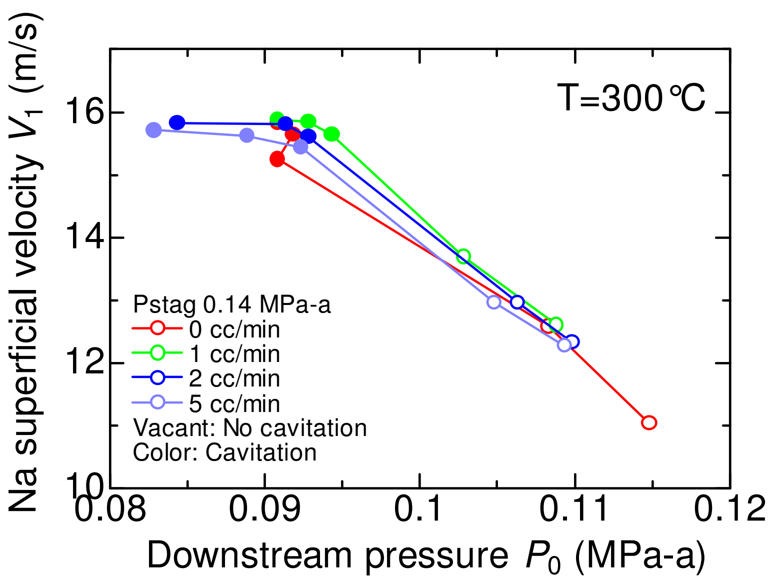

Fig. 4-22. Na superficial velocity as a function of downstream pressure at 300°C (Pstag: 0.14 MPa-a)

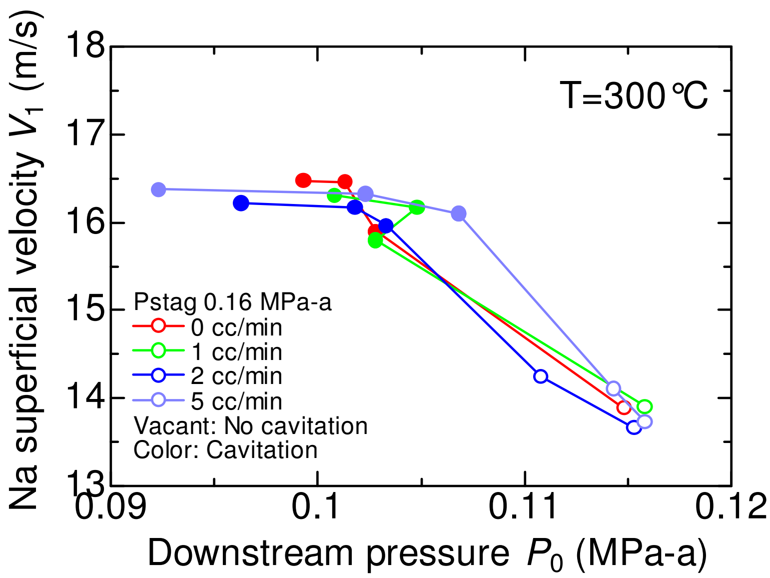

Fig. 4-23. Na superficial velocity as a function of downstream pressure at 300°C (Pstag: 0.16 MPa-a)

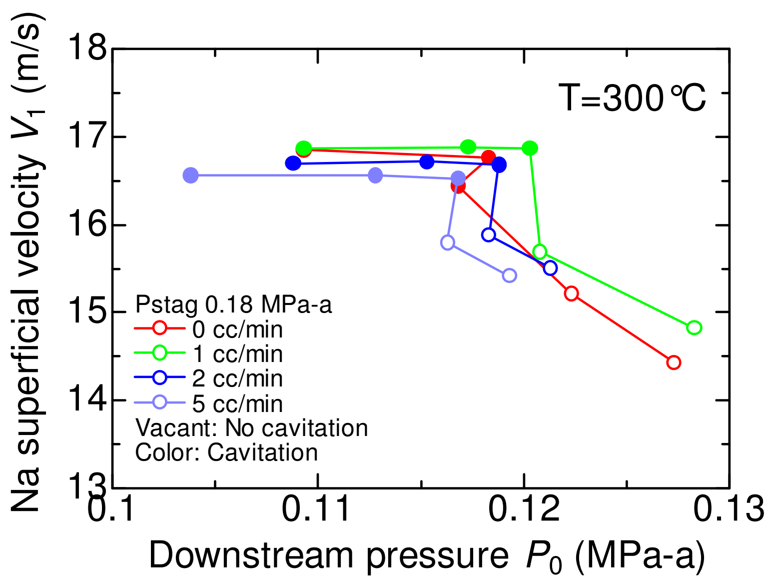

Fig. 4-24. Na superficial velocity as a function of downstream pressure at 300°C (Pstag: 0.18 MPa-a)

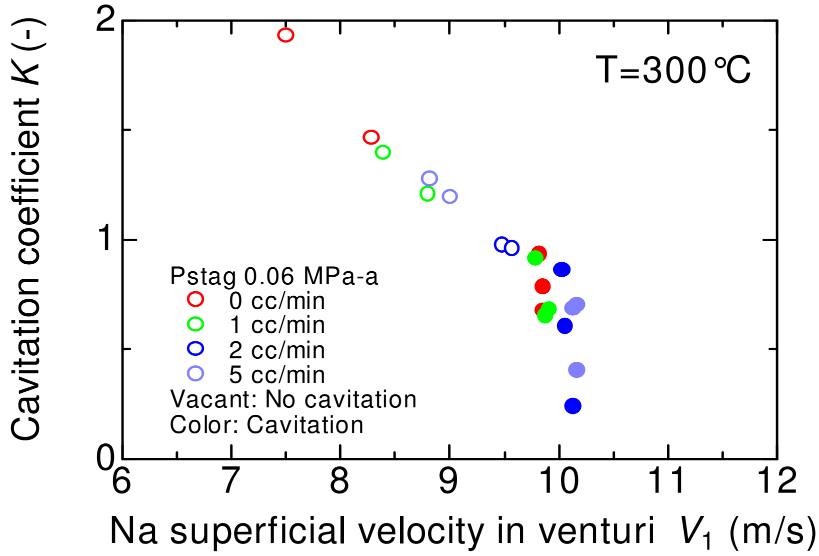

Fig. 4-25. Cavitation coefficient as a function of Na superficial velocity at 300°C (Pstag: 0.06 MPa-a)

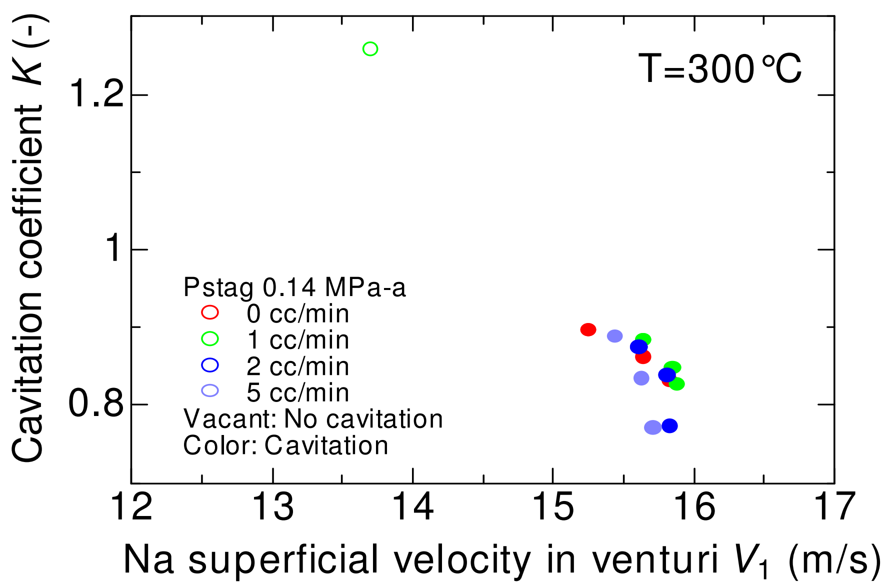

Fig. 4-26. Cavitation coefficient as a function of Na superficial velocity at 300°C (Pstag: 0.14 MPa-a)

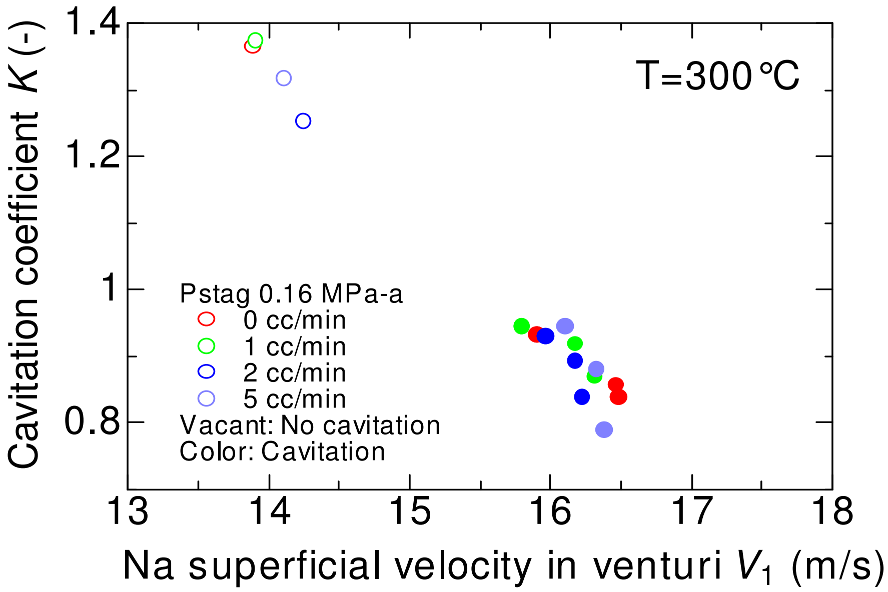

Fig. 4-27. Cavitation coefficient as a function of Na superficial velocity at 300°C (Pstag: 0.16 MPa-a)

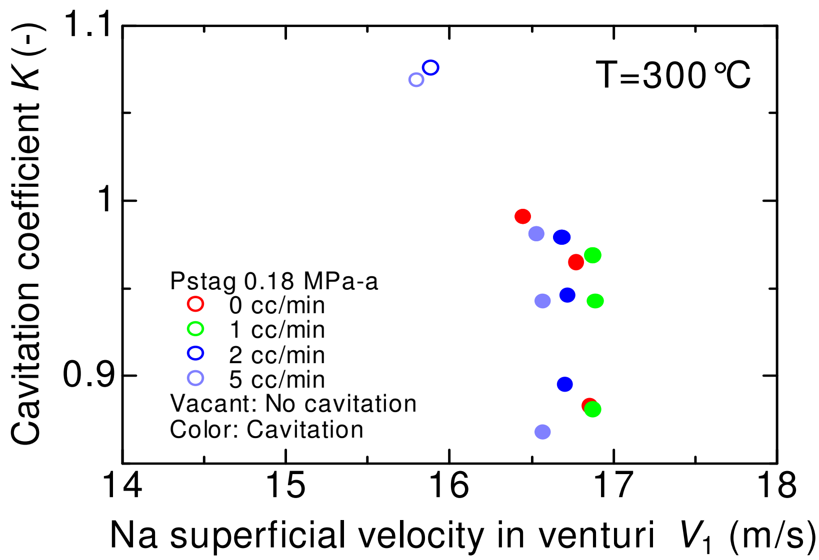

Fig. 4-28. Cavitation coefficient as a function of Na superficial velocity at 300°C (Pstag: 0.18 MPa-a)

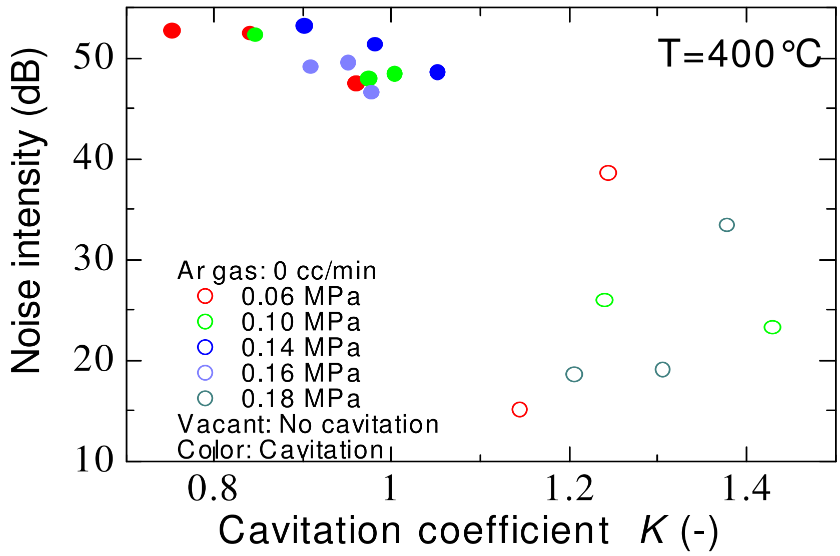

Fig. 4-29. Noise intensity as a function of cavitation coefficient at 400°C (Ar: 0 cc/min)

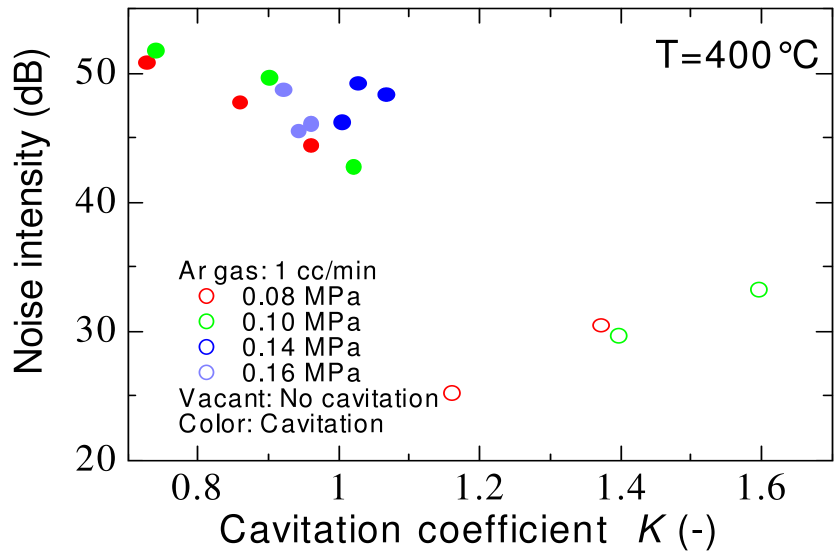

Fig. 4-30. Noise intensity as a function of cavitation coefficient at 400°C (Ar: 1 cc/min)

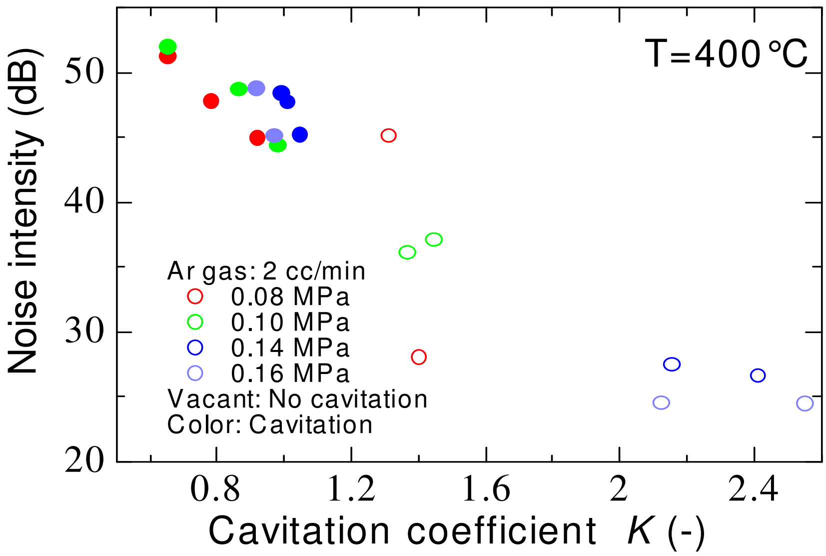

Fig. 4-31. Noise intensity as a function of cavitation coefficient at 400°C (Ar: 2 cc/min)

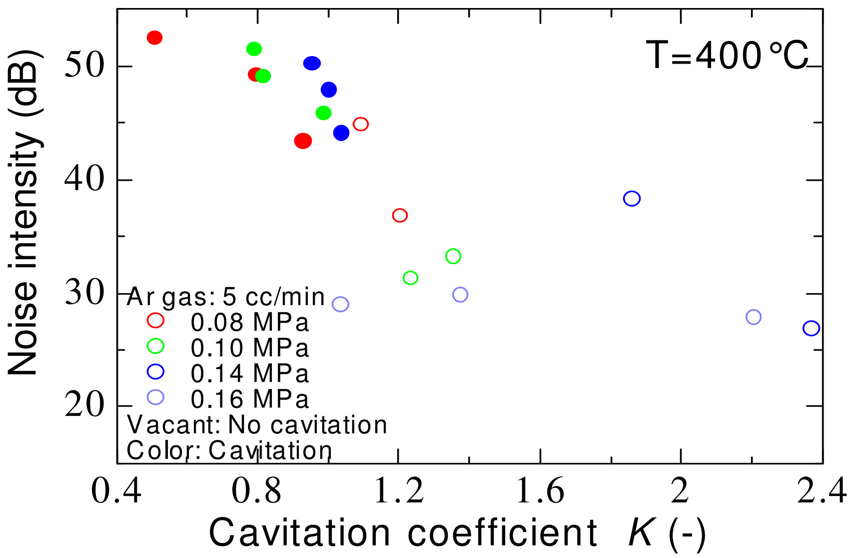

Fig. 4-32. Noise intensity as a function of cavitation coefficient at 400°C (Ar: 5 cc/min)

Fig. 4-25 to 4-28 show another results of cavitation experiment (cavitation coefficient as a function of sodium superficial velocity) at 300°C. The results show that the sodium superficial velocity starts to increase when the cavitation coefficient approaches unity. The sodium superficial velocity begins to saturate when the cavitation coefficient decreases below unity. The argon gas injection into the loop has no effect at the non-cavitation condition (cavitation coefficient above unity) and cavitation condition (cavitation coefficient below unity).

Fig. 4-29 to 4-32 show the results of the noise intensity as a function of cavitation coefficient at 400°C, argon gas injection of 0-5 cc/min and stagnant pressure of 0.06-0.18 MPa-a. The results show similarity with those obtained at 300°C. The noise intensity at the developed-cavitation condition becomes saturated with the magnitude of around 50 dB.

The results shown in Fig. 4-33 to 4-44 (noise intensity as a function of frequency) also has similarity with the results at 300°C, except at 0.16 MPa-a and argon gas flow rate of 5 cc/min in which there are no occurrences of cavitation (the maximum voltage level of electromagnetic flow rate meter). The noise intensity at 400°C and developed-cavitation condition is roughly around -40 dB.

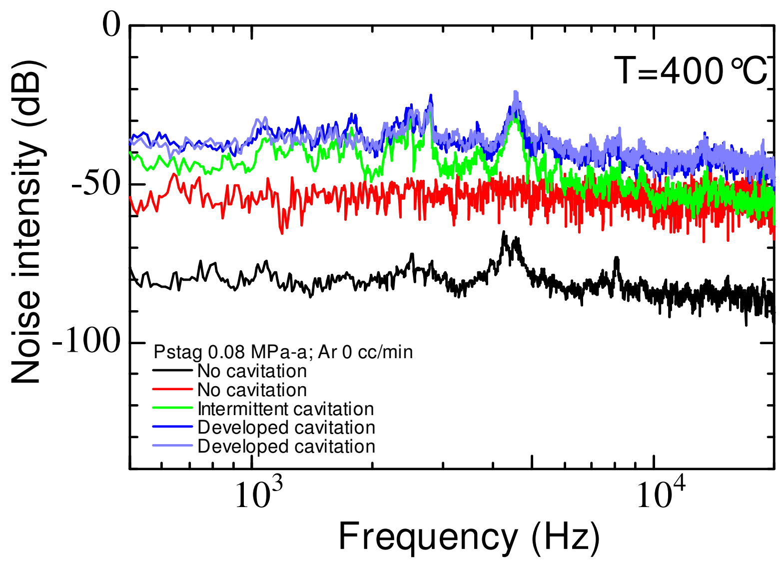

Fig. 4-33. Noise intensity as a function of frequency at 400°C
(Pstag: 0.08 MPa-a, Ar: 0 cc/min)

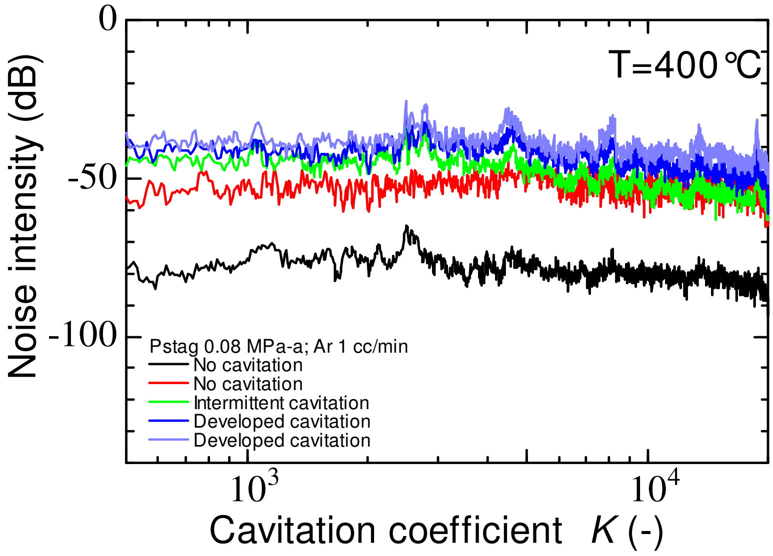

Fig. 4-34. Noise intensity as a function of frequency at 400°C
(Pstag: 0.08 MPa-a, Ar: 2 cc/min)

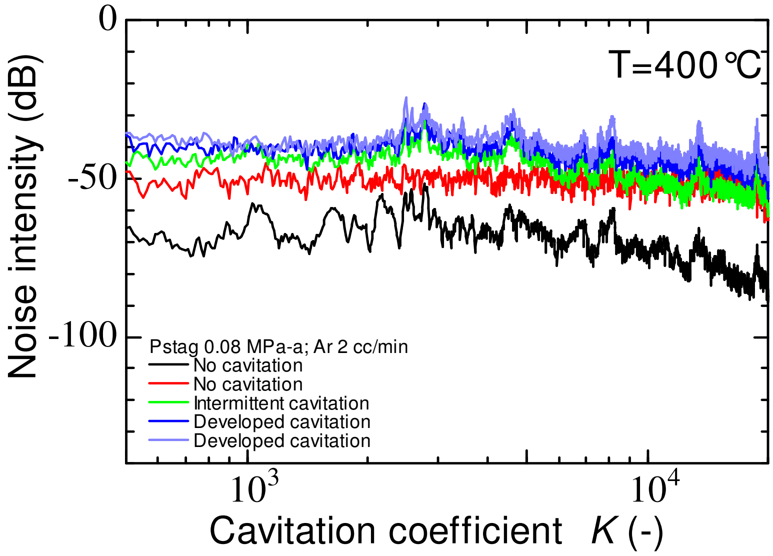

Fig. 4-35. Noise intensity as a function of frequency at 400°C
(Pstag: 0.08 MPa-a, Ar: 2 cc/min)

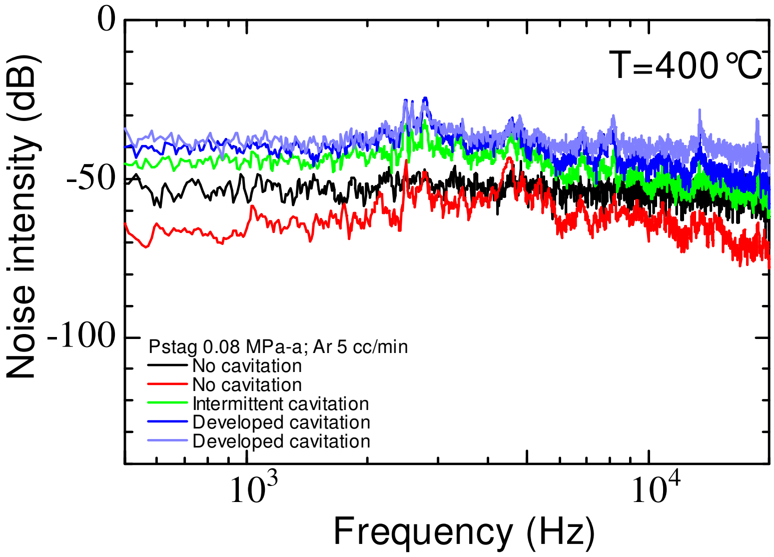

Fig. 4-36. Noise intensity as a function of frequency at 400°C
(Pstag: 0.08 MPa-a, Ar: 5 cc/min)

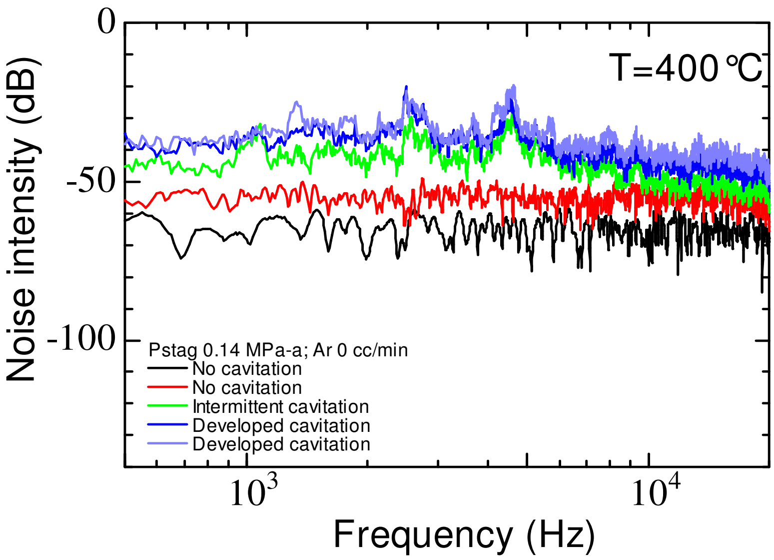

Fig. 4-37. Noise intensity as a function of frequency at 400°C
(Pstag: 0.14 MPa-a, Ar: 0 cc/min)

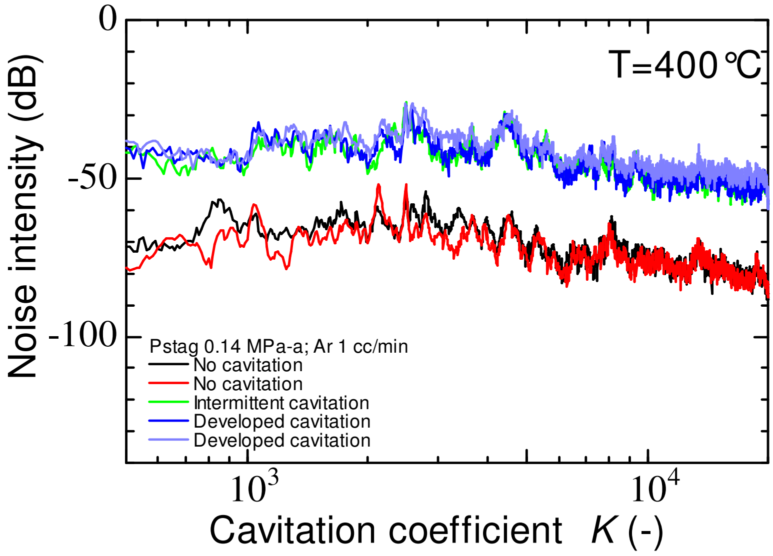

Fig. 4-38. Noise intensity as a function of frequency at 400°C

(Pstag: 0.14 MPa-a, Ar: 1 cc/min)

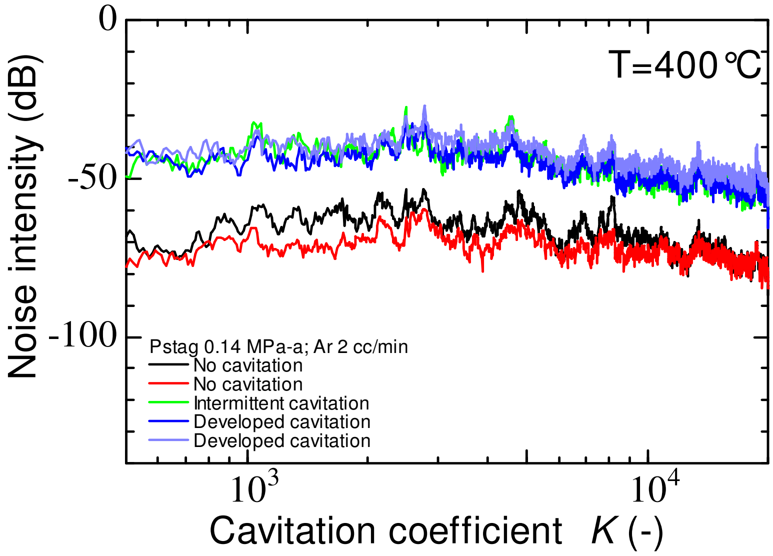

Fig. 4-39. Noise intensity as a function of frequency at 400°C

(Pstag: 0.14 MPa-a, Ar: 2 cc/min)

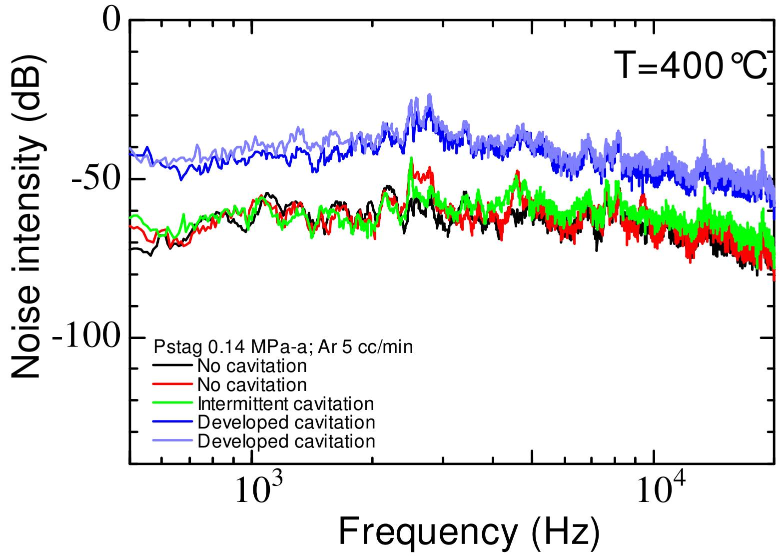

Fig. 4-40. Noise intensity as a function of frequency at 400°C
(Pstag: 0.14 MPa-a, Ar: 5 cc/min)

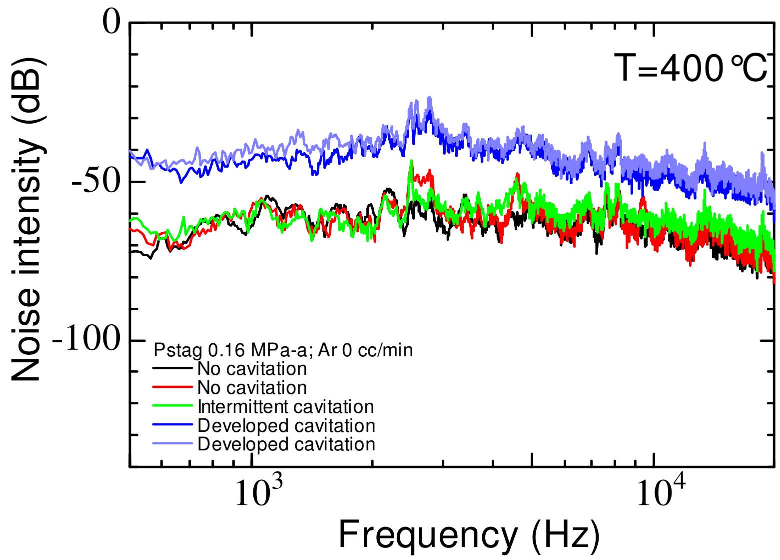

Fig. 4-41. Noise intensity as a function of frequency at 400°C
(Pstag: 0.16 MPa-a, Ar: 0 cc/min)

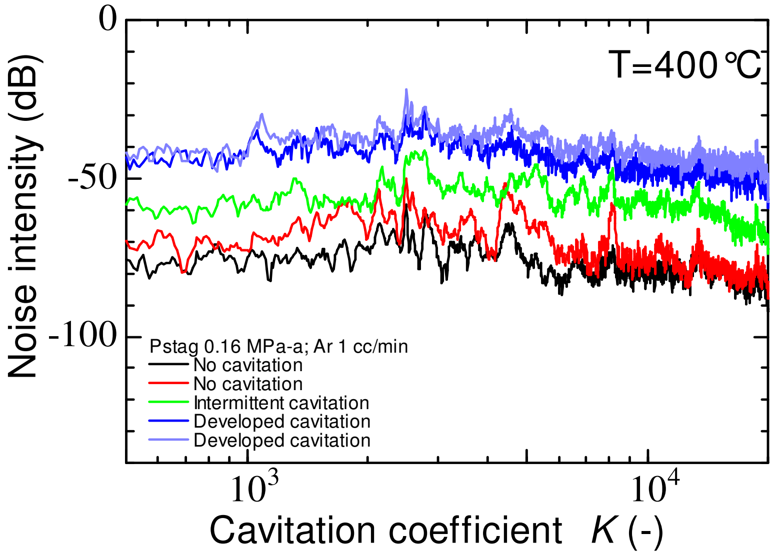

Fig. 4-42. Noise intensity as a function of frequency at 400°C
(Pstag: 0.16 MPa-a, Ar: 1 cc/min)

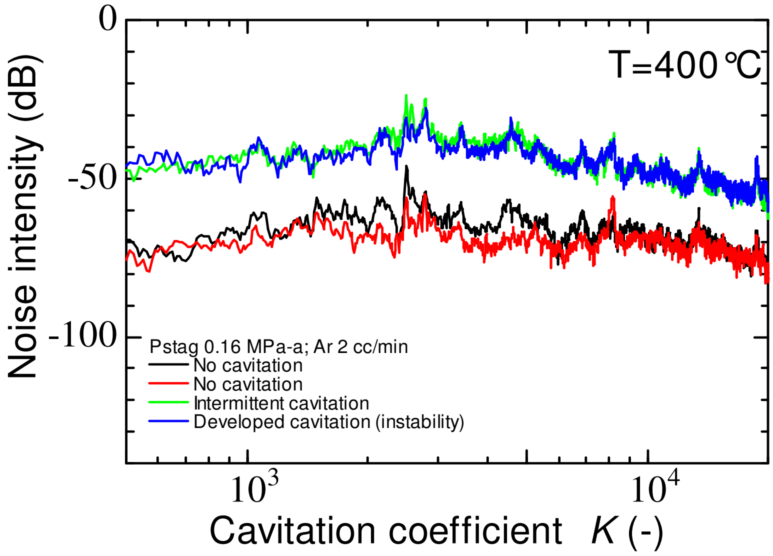

Fig. 4-43. Noise intensity as a function of frequency at 400°C
(Pstag: 0.16 MPa-a, Ar: 2 cc/min)

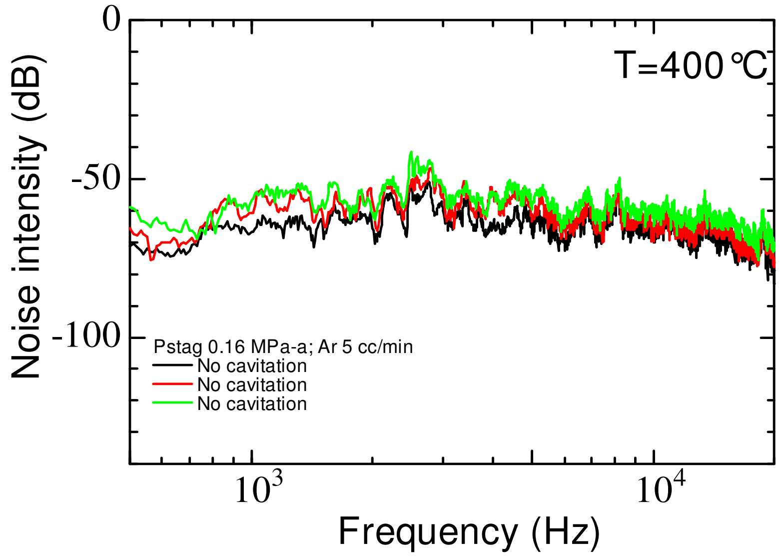

Fig. 4-44. Noise intensity as a function of frequency at 400°C

(Pstag: 0.16 MPa-a, Ar: 5 cc/min)

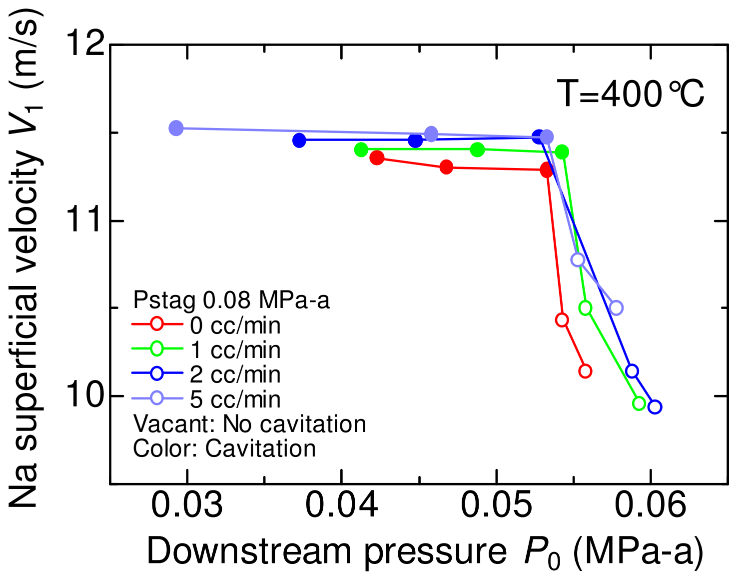

Fig. 4-45. Na superficial velocity as a function of downstream pressure at 400°C

(Pstag: 0.08 MPa-a)

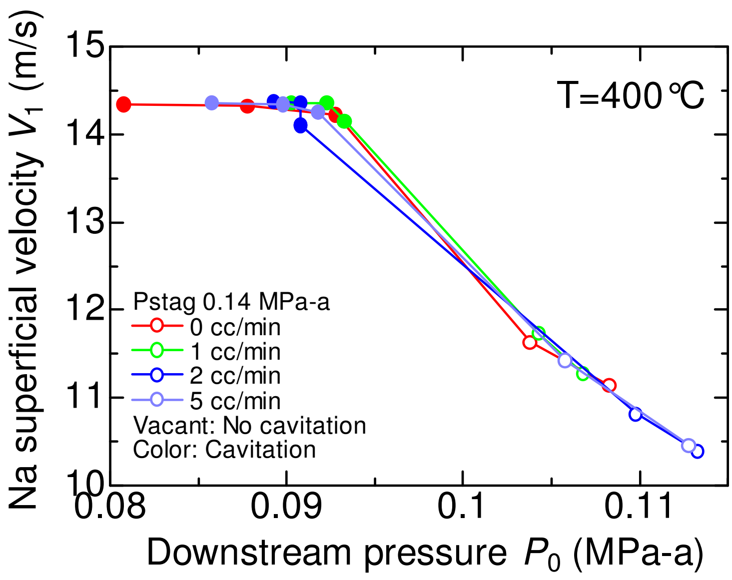

Fig. 4-46. Na superficial velocity as a function of downstream pressure at 400°C (Pstag: 0.14 MPa-a)

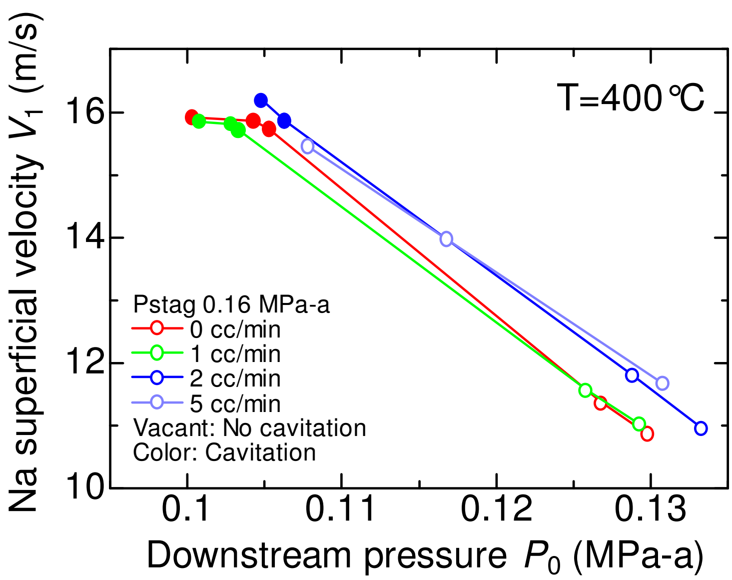

Fig. 4-47. Na superficial velocity as a function of downstream pressure at 400°C (Pstag: 0.16 MPa-a)

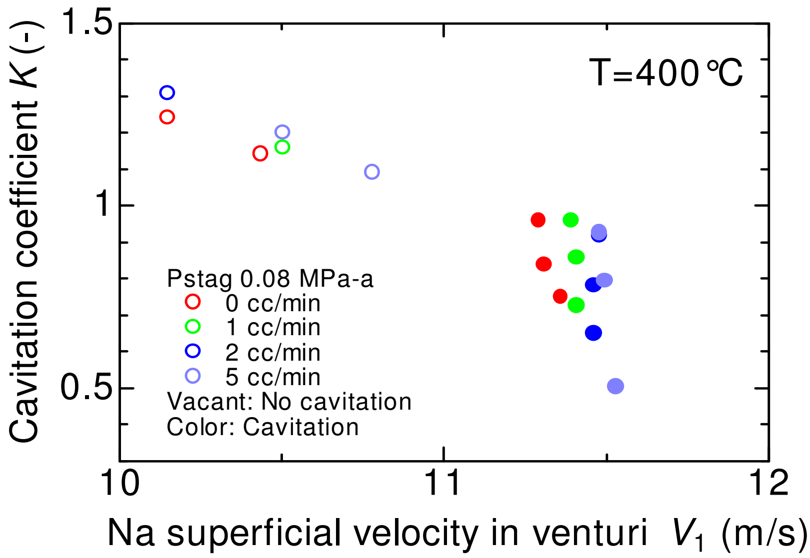

Fig. 4-48. Cavitation coefficient as a function of Na superficial velocity at 400°C (Pstag: 0.08 MPa-a)

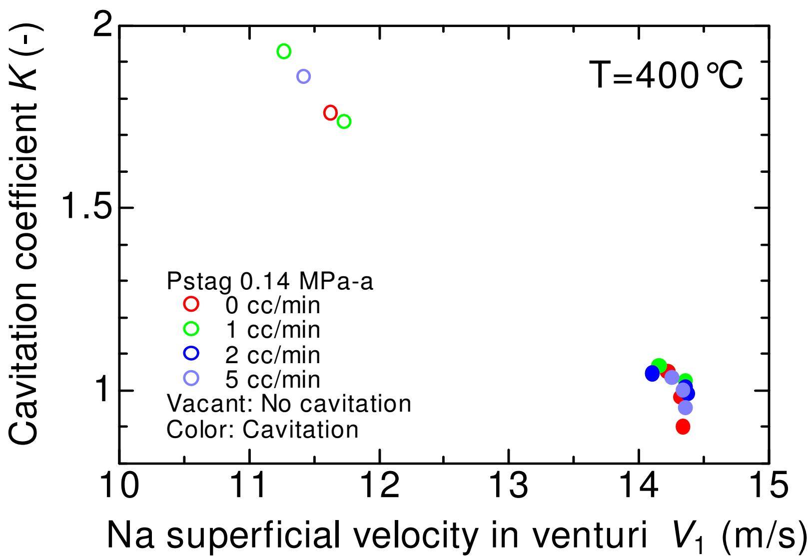

Fig. 4-49. Cavitation coefficient as a function of Na superficial velocity at 400°C (Pstag: 0.14 MPa-a)

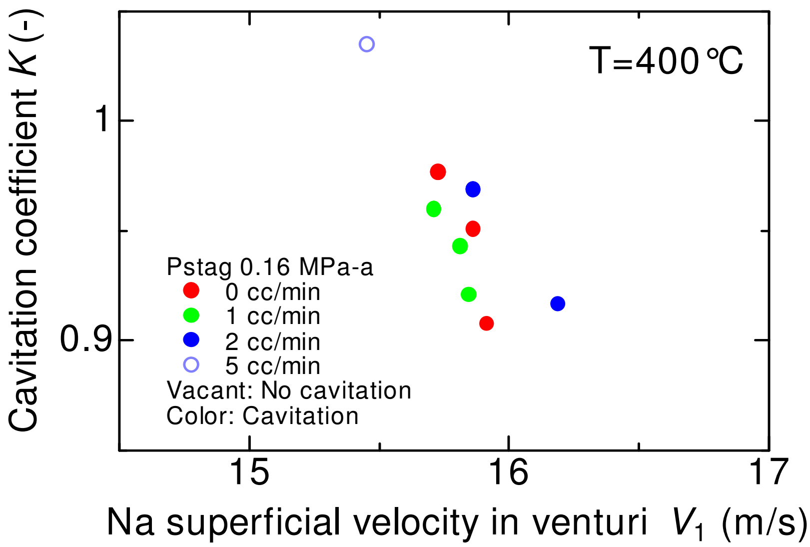

Fig. 4-50. Cavitation coefficient as a function of Na superficial velocity at 400°C (Pstag: 0.16 MPa-a)

Fig. 4-45 to 4-47 show the results of sodium superficial velocity as a function of downstream static pressure obtained at 400°C. The results obtained at 400°C show the similar trend as those obtained at 300°C (Fig. 4-21 to 4-24). At 0.08 MPa-a, the saturated sodium superficial velocity in the venturi is around 11.5 m/s. The velocity then increase to around 14.5 and 16 m/s at 0.14 MPa-a and 0.16 MPa-a, respectively. Also at 400°C, the injection of the argon gas in the flowing sodium loop has no significant effect on the liquid sodium superficial velocity at 0.08, 0.14 and 0.16 MPa-a.

Fig. 4-48 to 4-50 show the similar results with those obtained at 300°C. The decrease of the cavitation coefficient has a relation to the increase of the liquid sodium superficial velocity in venturi. The velocity starts to saturate when the cavitation coefficient is below unity (developed-cavitation condition). Also, the increase of the liquid sodium temperature from 300 to 400°C makes the cavitation phenomenon occur more easily at the same stagnant pressure (lower velocity). It might be caused by the increase of vapor pressure in liquid sodium.

The small effect of the argon gas injection into the flowing liquid sodium loop might be explained in this way. During the operation of the sodium loop, the velocity of the liquid sodium was very high. This high velocity was needed in order to create very high velocity and low static pressure in the venturi. The cavitation bubbles started to form in the venturi when the static pressure is less than the vapor pressure of the liquid sodium at some point of experimental temperature. The argon gas bubbles formed by the injection of argon gas into the high velocity liquid sodium loop would change in shape and size when they grew and passed through the venturi and collapsed at the downstream region due to pressure gradients, boundary layers, separation and turbulence. The change of bubbles size and shape into smaller ones would reduce the noise intensity during the collapse conditions at the downstream region. Furthermore, smaller cavitation bubbles would create mute cavitation noise when they collapse due to attenuation by the fluid and the wall; hence the noise intensity remains unchanged. In other case, the bubble radius could be less than the critical bubble radius. According to Brennen [25], a bubble will become unstable, growth and cavitate if the radius is larger than theoretical bubble radius, R, while that with the smaller radius will not affected.

4.3. Conclusion

Liquid sodium cavitation experiment in the venturi with the injection of argon gas has been performed and some conclusions could be drawn, i.e.

1) Cavitation starts to occur when the value of cavitation coefficient is approximately equal to unity.

2) The noise intensity created by the collapse of cavitation bubbles at 300° and 400°C is similar.

3) The magnitude of the noise intensity at developed-cavitation condition and temperature of 300° and 400°C remain unchanged for every stagnant pressure and injected argon gas flow rate.

4) The magnitude of the noise intensity rises to a higher value for all frequencies, ranging from 0-20,000 Hz.

5) The cavitation phenomenon is similar with the choked/critical flow phenomenon. The decrease of the downstream static pressure during cavitation does not change the liquid sodium superficial velocity (it remains relatively constant).

6) The liquid sodium superficial velocity is affected by the stagnant pressure. The higher the stagnant pressure, the higher the velocity is. Also, the increase of the liquid sodium temperature from 300 to 400°C makes the cavitation phenomenon occur more

easily at the same stagnant pressure.

7) The injection of argon gas in the flowing liquid sodium loop does not change the noise intensity created by the collapse of the cavitation bubbles significantly. It might be explained by the change in size and shape of the argon gas bubbles when passed through the venturi and collapsed downstream.

CHAPTER V

Water Cavitation Experiment in Venturi

5.1. Introduction

Cavitation phenomenon in liquid sodium is hard to be visualized since sodium is not transparent. In order to visualize the phenomenon of cavitation in liquid sodium, water is used as the simulant fluid. Water itself has the density close to the liquid sodium and its transparent effect makes it possible to visualize the phenomenon of cavitation that occurs inside the venturi. Since cavitation phenomenon is a very fast phenomenon, a high speed video camera or camera is required to record the image.

5.2. Result and Discussion

Fig. 5-1 shows the resonance frequency spectrum during the hit test conducted at stagnant pressure of 0.06 MPa-a and water temperature of 10°C. The spectrum shows multiple resonance peaks for frequencies lower than 10,000 Hz.

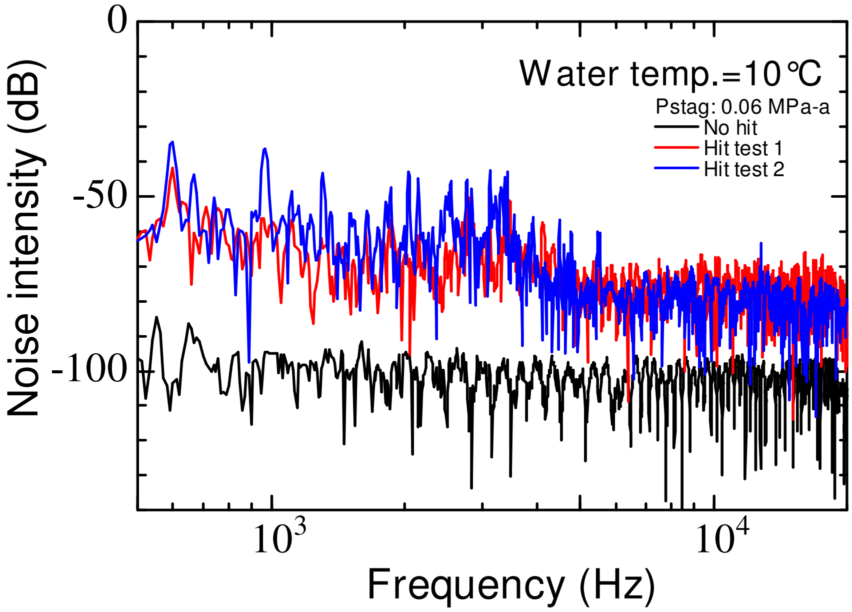

Fig. 5-1. Resonance frequency of the water cavitation test section

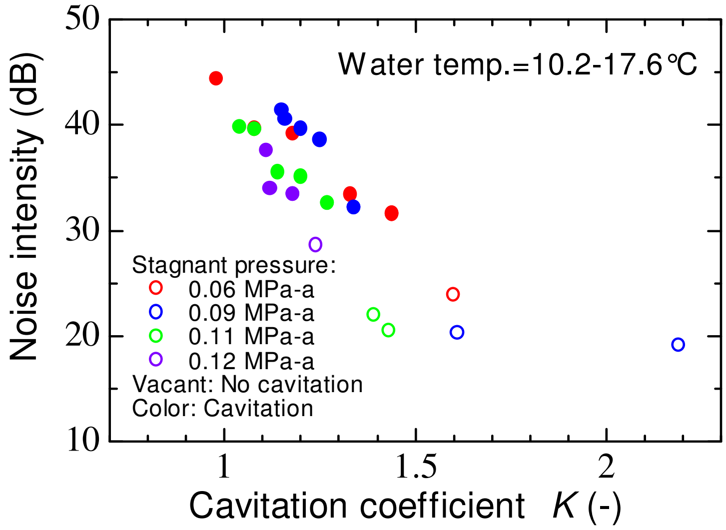

Fig. 5-2. Noise intensity as a function of cavitation coefficient for water

The results of cavitation experiment using water in venturi are shown in Fig. 5-2 to 5-10. Fig. 5-2 shows the result of noise intensity as a function of cavitation coefficient for water stagnant pressure ranging from 0.06-0.12 MPa-a. From the figure it can be shown that during the no cavitation condition (shown by the vacant symbol) the noise intensity is very low (around 20 dB). The noise starts to increase suddenly at around 40 dB when cavitation starts to occur inside the venturi. This condition is known as intermittent cavitation because the cavitation phenomenon is unstable (occur intermittently). In water, cavitation starts to occur around K=1.5. This value is larger than the cavitation experiment conducted using liquid sodium (K is around 1.1) and from the theoretical prediction (K=1). The noise intensity produced by the collapse of cavitation bubbles in water during developed cavitation condition is a little bit smaller than that using sodium (around 43 dB in sodium compared with around 40 dB in water). The different stagnant pressure of water loop does not affect the noise intensity produced during cavitation condition. The change of water temperature from 10.2-17.6°C was caused by the pump operation.

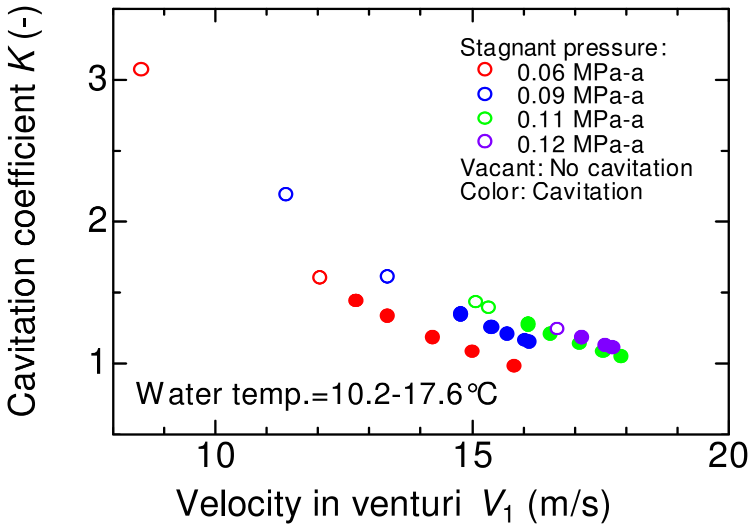

Fig. 5-3. Cavitation coefficient K as a function of venturi velocity for water

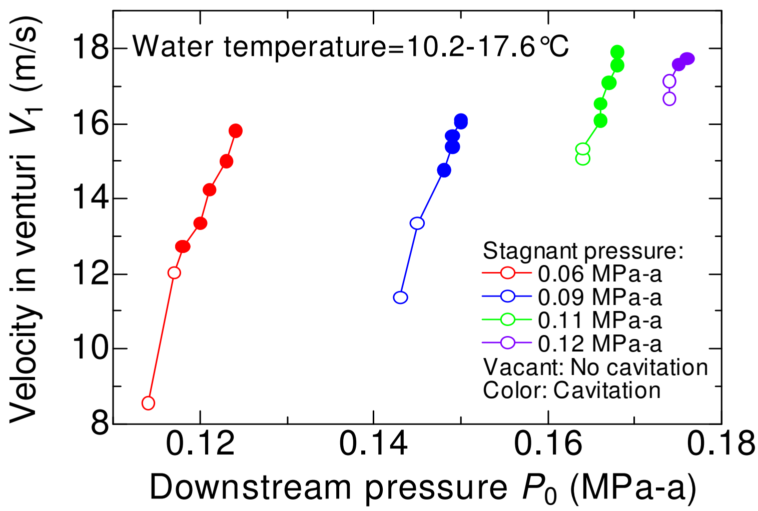

Fig. 5-4. Velocity in venturi as a function of downstream pressure

Fig. 5-3 and 5-4 show the result of cavitation coefficient K as a function of venturi velocity and water velocity in venturi as a function of downstream pressure for water. In Fig. 5-3 the result shows $1/V_1^2$ relation between cavitation coefficient and water superficial velocity in venturi when the condition changes from no cavitation condition to the developed cavitation condition. This result indicates that chocking/critical like phenomena as recorded using liquid sodium did not occur for venturi cavitation in water. It might be caused by the head of the water loop apparatus that collapses the cavitation bubbles in the downstream region and prevents them to be carried under into the pump. The result shows that with the increase of the stagnant pressure in the water loop system, the cavitation coefficient at the incipient/onset cavitation condition also changes. The value changes from around 1.4 at 0.06 MPa-a to around 1.2 at 0.12 MPa-a. It indicates that at high pressure condition, the formation of cavitation bubbles is suppressed and cavitation starts to occur at lower cavitation coefficient and higher velocity, similar with the result obtained using liquid sodium.

Fig. 5-5 to 5-8 show the result of the experiment between noise intensity and frequency from 0.06-0.11 MPa-a. The results show that the noise intensity during cavitation tends to increase in the higher frequency region than at the lower one. These results are similar with the results obtained by using sodium but with a little bit lower intensity. The noise intensity (amplitude) variations for each spectrum (no cavitation, intermittent cavitation and developed cavitation) in water are higher compared to that in sodium. This might be caused be the intense vibrations of the water loop system and electrical noise of the measurement system.

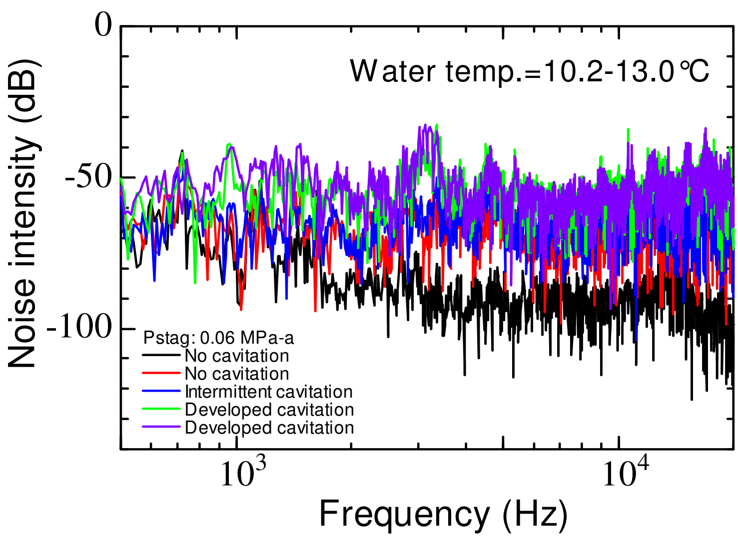

Fig. 5-5. Noise intensity as a function of frequency at 0.06 MPa-a for water

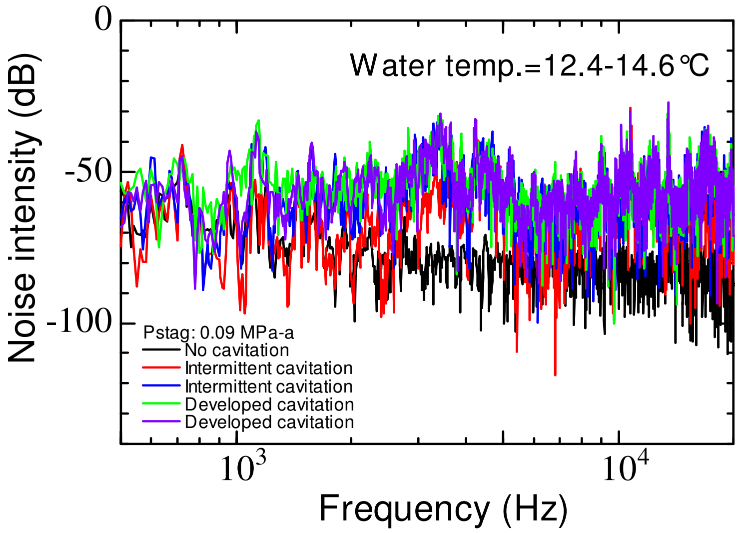

Fig. 5-6. Noise intensity as a function of frequency at 0.09 MPa-a for water

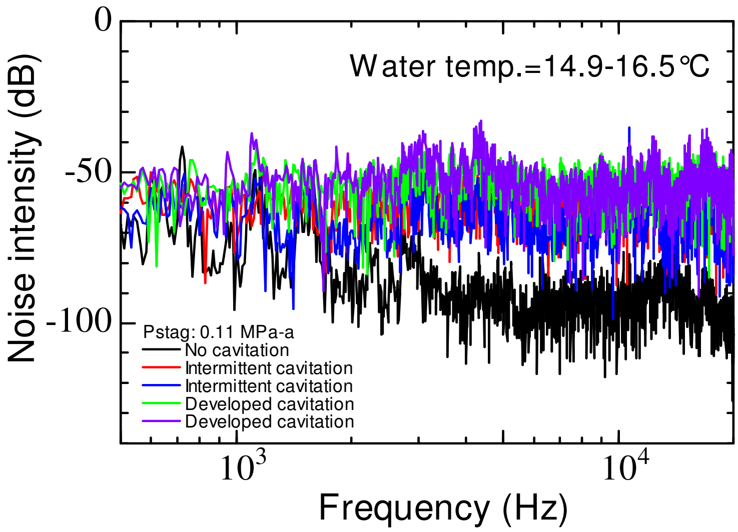

Fig. 5-7. Noise intensity as a function of frequency at 0.11 MPa-a for water

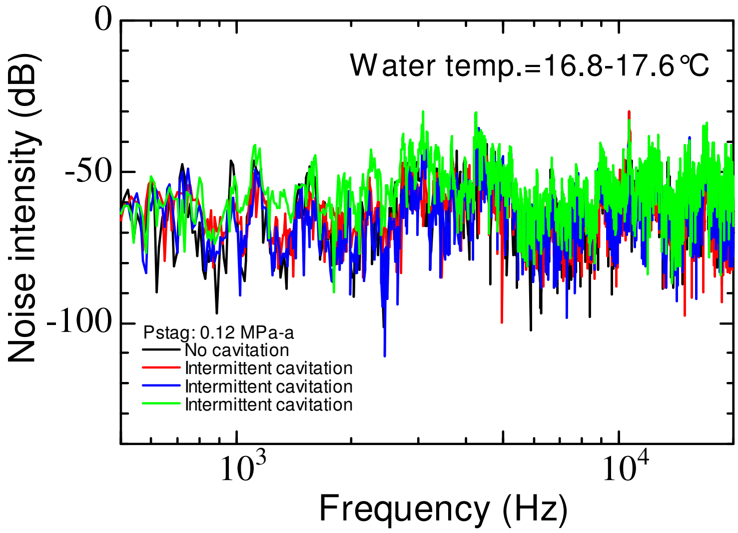

Fig. 5-8. Noise intensity as a function of frequency at 0.12 MPa-a for water

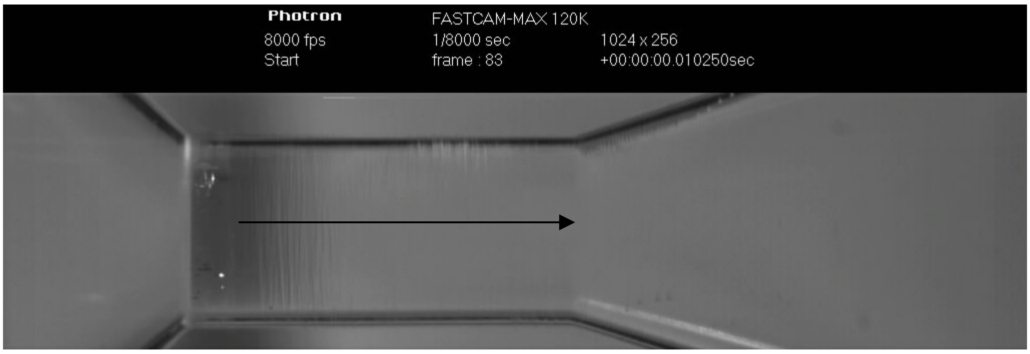

Fig. 5-9. High-speed picture of no cavitation condition (the flow is from left to right)

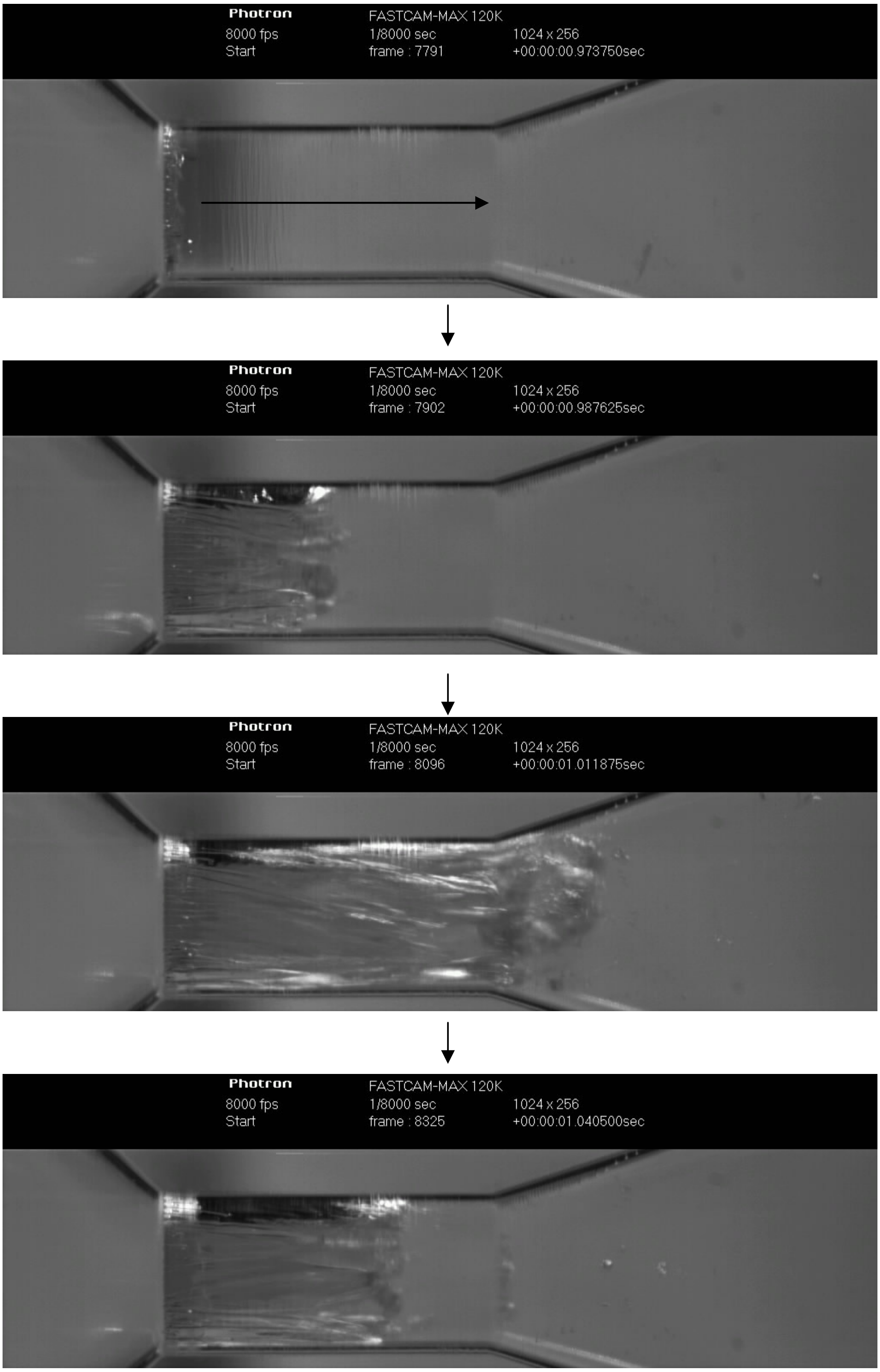

Fig. 5-10. High-speed pictures of intermittent cavitation condition

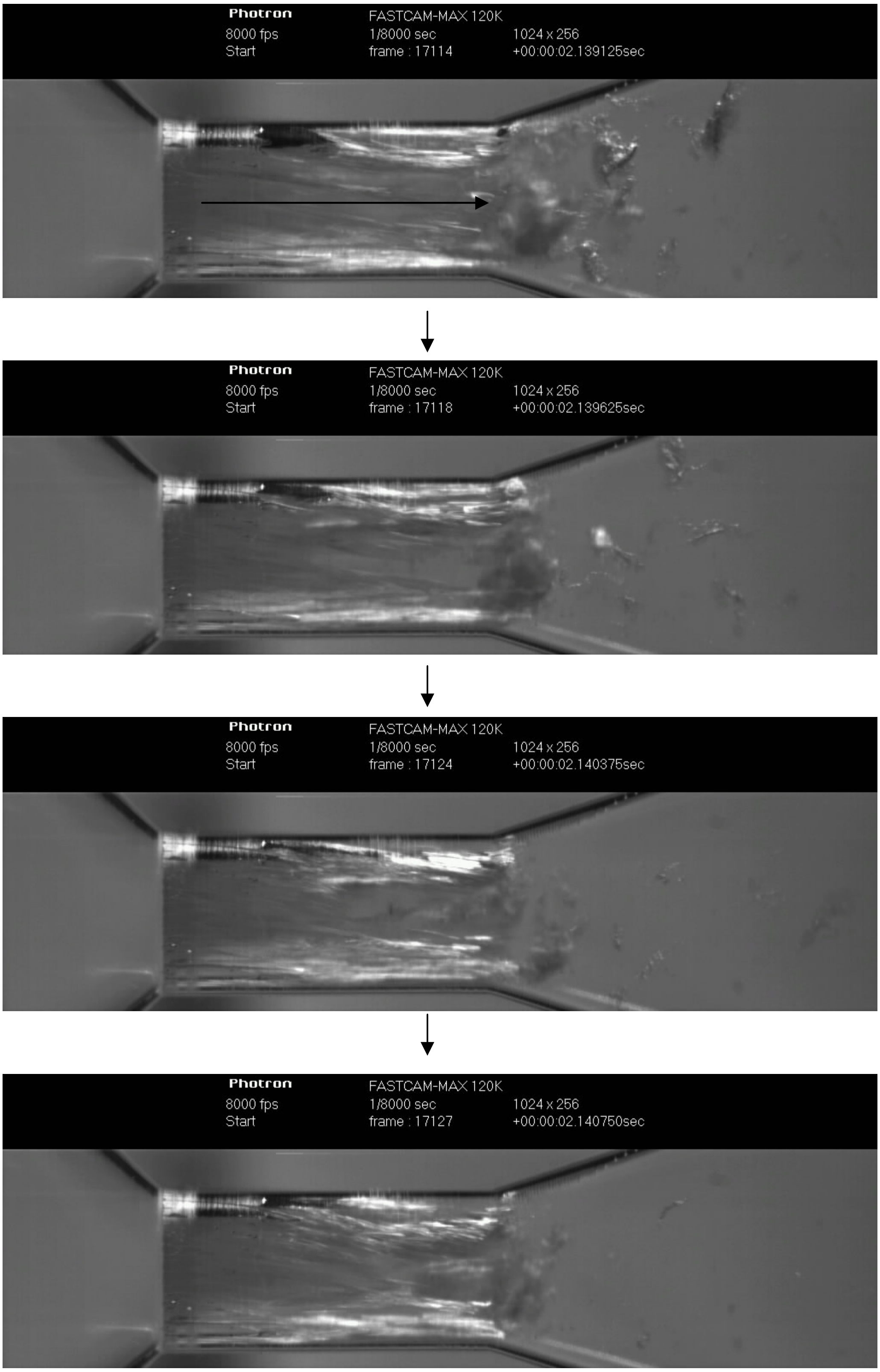

Fig. 5-11. High-speed pictures of developed cavitation condition

Fig. 5-9 shows the picture of the venturi test section obtained by the high-speed camera at 8,000 fps during the no cavitation condition. It shows a clear flow of water in the test section and no bubbles were formed. The direction of the flow is from left to right. Fig. 5-10 shows the intermittent cavitation phenomenon in the venturi region. Because of the high flow rate, some bubbles were formed at the inlet of the venturi. The bubbles were elongated to the flow direction creating a stream-like flow. When the elongated bubbles reach the outlet of the venturi, the bubbles were detached and collapsed at the downstream region. The elongated bubbles were not stable and could restore to their previous length. Fig. 5-11 shows the pictures of developed cavitation condition. The elongated bubbles formed during developed cavitation condition were stable and some large and small bubbles collapsed at the downstream region. Most of the bubbles that collapsed at the downstream region were not spherical and the collapse was observed far away from the venturi outlet. The non-spherical bubbles might be affected by the pressure gradient, boundary layers, turbulence and the collapse of other bubbles.

5.3. Conclusion

From the water cavitation experiment, it can be concluded that:

1) The cavitation coefficient K at the onset condition is higher compared with that using liquid sodium.
2) The stagnant pressure does not change the noise intensity produced by the bubbles collapse.
3) Cavitation tends to occur at higher frequency region than at the lower one.
4) The change of stagnant pressure affects the onset velocity in the venturi, hence change the cavitation coefficient K. The result shows exponential relation between cavitation coefficient and water velocity in venturi.
5) Observations using a high speed camera revealed that because of the high flow rate, some bubbles were formed at the inlet of the venturi. The bubbles were elongated to the flow direction creating a stream like flow. When the elongated bubbles reach the outlet of the venturi, the bubbles were detached and collapsed at the downstream region.
6) Most of the bubbles that collapsed at the downstream region were not spherical

and the collapse was observed far away from the venturi outlet. The non-spherical bubbles might be affected by the pressure gradient, boundary layers, turbulence and the collapse of other bubbles.

CHAPTER VI

Conclusion

Study on characteristics of sodium and water cavitation in flow contraction has been carried out. The onset of sodium cavitation without and with argon gas injection into the flowing liquid sodium loop and the result of cavitation experiment in water loop have been confirmed in Chapter III, IV and V, respectively. From this study, it could be concluded that:

1) The noise intensity produced by the collapse of cavitation bubbles in liquid sodium is a little bit higher compared with that in water. The onset cavitation coefficient K in liquid sodium is close to unity, while that in water is higher (around 1.5).
   a) In the liquid sodium cavitation experiment, the increase of liquid sodium temperature makes the cavitation phenomenon occur more easily at the same stagnant pressure.
   b) Increasing the stagnant pressure will increase the flow rate to start cavitation in the test section both for water and sodium.
2) The noise intensity tends to increase at higher frequency region at low temperature, but increase in both high and low frequency regions at high temperature.
3) The injection of argon gas into the flowing liquid sodium does not change the noise intensity at the onset and developed cavitation conditions. It might be explained by the change in size and shape of the argon gas bubbles when passed through the venturi and collapsed downstream.
4) The cavitation phenomenon in liquid sodium is similar with the critical/choked flow phenomenon. This phenomenon was not found in water cavitation experiment.
5) In the water cavitation experiment, the the growth and collapse of cavitation bubbles were not spherical. It might be affected by the pressure gradient, boundary layers, turbulence and the collapse of other bubbles.

References

[1] IEA (International Energy Agency), "World Energy Outlook 2008, Executive Summary," Paris, France, 2008.

[2] WEC (World Energy Council), "2007 Survey of Energy Resources," London, United Kingdom, 2007.

[3] PRIS (Power Reactor Information System), IAEA.

[4] U. S. DOE Nuclear Energy Research Advisory Committee and the Generation IV International Forum, "A Technology Roadmap for Generation IV Nuclear Energy Systems", December, 2002.

[5] IAEA (International Atomic Energy Agency), "Nuclear Technology Review 2007", Vienna, Austria, 2007.

[6] Roglans, J., T. Allen, M. Lineberry, "Sodium-cooled Fast Reactor (SFR) Systems", ANS winter meeting, Washington D. C., November 18, 2002.

[7] Chang, M. H., "Fast Reactor Technology Development Plans in Korea and Expectations for MONJU", The 4th Tsuruga International Energy Forum, Japan, 2004.

[8] P. Courbiere, "An acoustic Method for Characterizing the Onset of Cavitation in Nozzles and Pumps", International Symposium on Cavitation Inception, pp. 137-143, 1984.

[9] S. R. Bistafa, "Noise Generated by Cavitation in Orifice-Plates with Some Gaseous Effects", International Symposium on Cavitation and Multiphase Flow Noise, pp. 41-52, 1986.

[10] P. Testud, P. Mussou, A. Hirschberg, Y. Auregan, "Noise Generated by Single-Hole and Multi-Hole Orifices in A Water Pipe", Journal of Fluid and Structures 23, pp. 163-189, 2007.

[11] S. L. Ceccio, C. E. Brennen, "Observations of the Dynamics and Acoustics of Traveling Bubble Cavitation", Journal of Fluid Mechanic 233, pp. 633-660, 1991.

Stanley G. Young, James R. Johnston, "Effect of Cover Gas Pressures on Accelerated

[12] Cavitation Damage in Sodium", NASA TN D-4235, November 1967.

[13] Timo Koivula, "On Cavitation in Fluid Power", Proceeding of 1st FPNI-PhD Symposium, Hamburg, pp. 371-382, 2000.

[14] Ono Sokki NP Series Accelerometers Catalogue.

[15] Giles, R. V., J. B. Evett, C. Liu, “Schaum`s Theory and Problems, Fluid Mechanics and Hydraulics, 3rd Edition”, McGraw-Hill, Inc., 1994.

[16] Ashcroft GC-51 Calibration Data, Nagano Keiki Co., Ltd.

[17] Till, C. E., Y. I. Chang, W. H. Hannum, "The Integral Fast Reactor-An Overview." Progress in Nuclear Energy 31 (1-2), pp. 3-11, 1996.

[18] Kiryushin, A. *et al*., Proceedings of the Tenth International Conference on Nuclear Engineering, American Society of Mechanical Engineers, April 14-18, paper 10-22405, 2002.

[19] King, R. W., D. L. Porter, Proceedings of the Tenth International Conference on Nuclear Engineering, American Society of Mechanical Engineers, April 14-18, paper 10-22524, 2002.

[20] Fitch, E. C., “Cavitation Wear in Hydraulic Systems,” Practicing Oil Analysis Magazine, September, 2002.

[21] Brennen, C. E., “Cavitation and Bubble Dynamics,” Oxford University Press, 1995.

[22] Kale, R. D. *et al*., “Developments in Sodium Technology,” Current Science 86 (5), pp. 668-675, 2004.

[23] Govindaraj, G., C. Raju, R. D. Kale, G. Vaidyanathan, “Gas Entrainment in Surge Tank of Liquid Metal Fast Breeder Reactors”, JNST, 30(7), pp. 712-716, July 1993.

[24] Vaidyanathan, G., K. Swaminathan, “Techniques for Investigation of Gas Entrainment”, IGC Newsletter, Vol. 20, 1994.

[25] Brennen, C. E., “Fundamentals of Multiphase Flows,” Cambridge University Press, 2005.

Appendix A.

Schematic of water loop apparatus for water cavitation experiment.

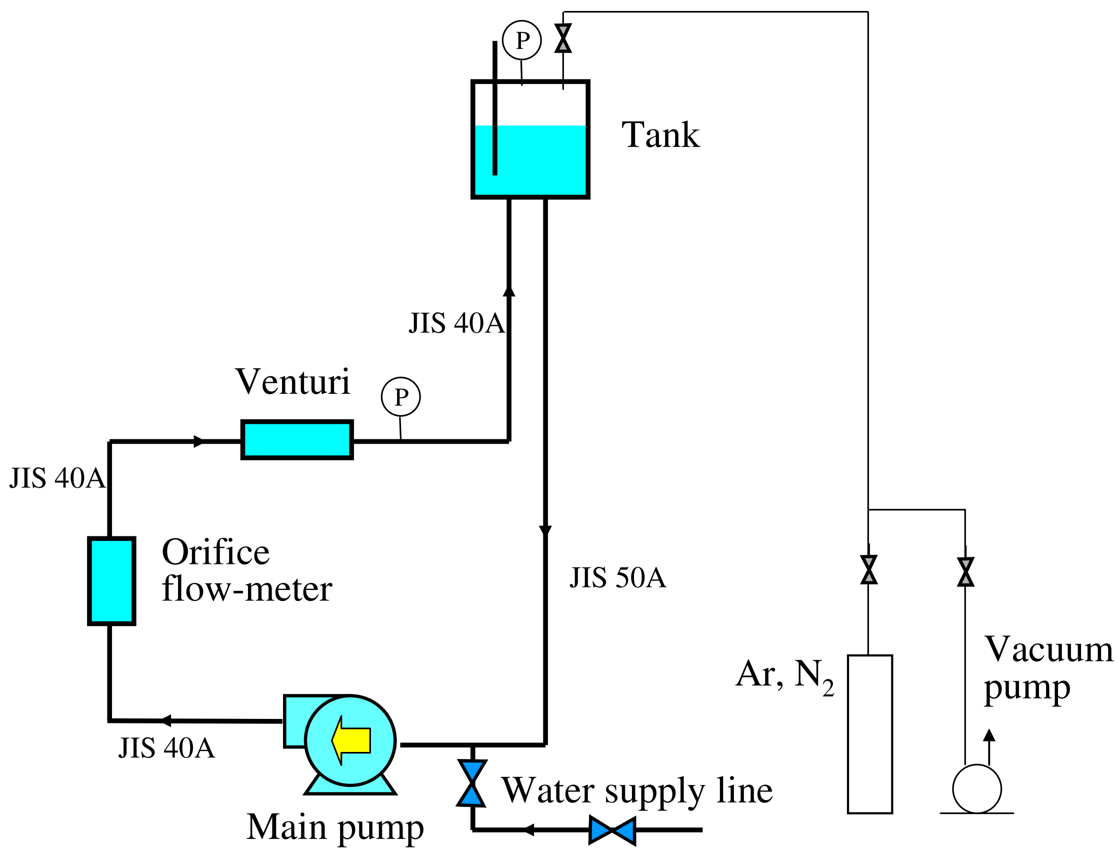

Appendix B.

Schematic of sodium loop apparatus for sodium cavitation experiment.

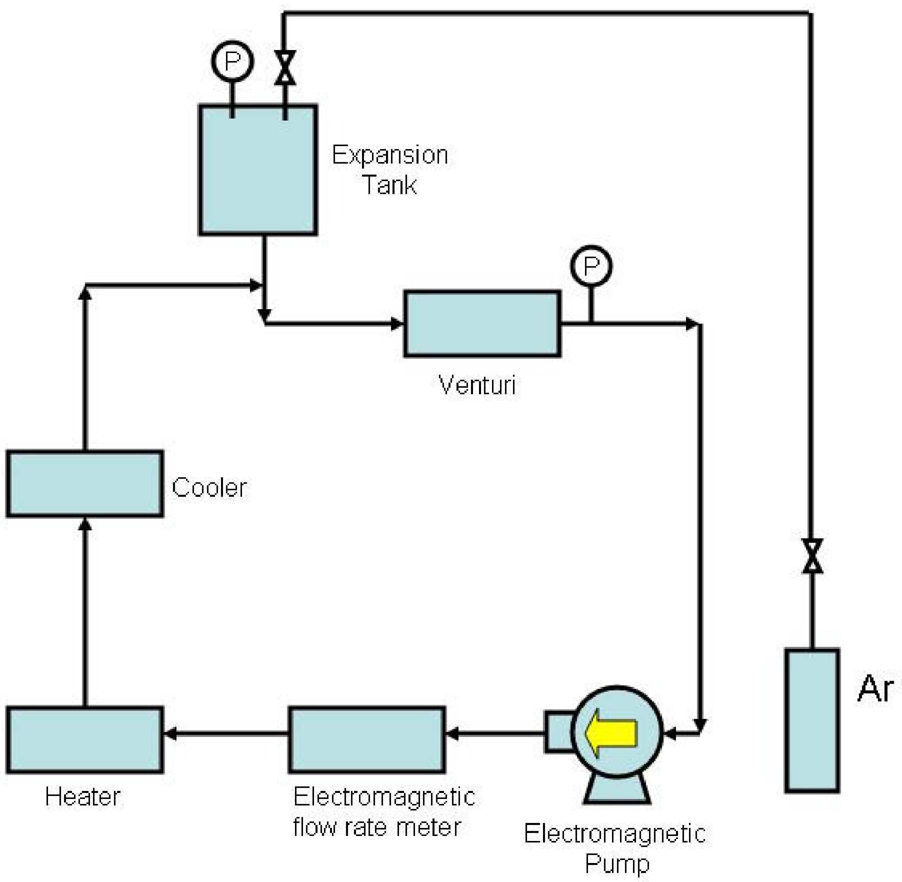

Acknowledgement

The author would like to express his sincere gratitude to:

1) Assoc. Prof. Minoru Takahashi for his valuable support and discussion as a master thesis supervisor.
2) Prof. Yoshio Yoshizawa, Prof. Hisashi Ninokata, Prof. Masanori Aritomi and Assoc. Prof. Yukitaka Kato for their valuable comments and questions during my master thesis presentation.
3) Ass. Prof. Masamichi Nakagawa, Mr. Kuniaki Miura and Mr. Makoto Asaba for their encouragement and kindness during the sodium cavitation experiment at Sukegawa Electric, Co. Ltd..
4) Mr. Abu Khalid Rivai, Miss Eriko Yamaki, Mr. Asril Pramutadi, Mr. Sa Rongyuan, Miss Xinhua Zhou for their warmth hospitality as members of Takahashi`s Lab..
5) My senior and close friend Mr. Muhammad Kunta Biddinika for encouraging me when I am awfully low.
6) All my Indonesian friends in Indonesia and Tokyo for cherishing my study life.
7) My beloved sister and brothers, Tafriyandi, Novita and Ardhy for being my good sister and brothers during my stay in Indonesia.
8) My beloved parents, my father Tarmidi and my mother Arijani for their continuous praying during my study. Thank you for trusting in me.
9) All of my family in Surabaya, Indonesia for their encouragement and pray, especially my grandmother, Pani.